Title

Arabidopsis thaliana rosette growth habit is a photomorphogenic trait controlled by the TALE homeodomain protein ATH1 and involves TOR kinase

Authors

Shahram Shokrian Hajibehzad[1], Savani S. Silva[1], Niels Peeters[1], Evelien Stouten[1], Guido Buijs[1], Sjef Smeekens[1], and Marcel Proveniers[1]*

Affiliations

[1]Molecular Plant Physiology, Department of Biology, Science4Life, Utrecht University, Padualaan 8, Utrecht, 3584 CH, The Netherlands.

* Correspondence: Marcel Proveniers, m.proveniers@uu.nl

Contact

Marcel Proveniers, m.proveniers@uu.nl

Running title

Rosette habit is a photomorphogenic trait controlled by ATH1

Abstract

Here, we demonstrate that Arabidopsis rosette habit is a *bona fide* photomorphogenic trait controlled by the homeodomain protein ATH1. In light, *ATH1* expression at the SAM is induced by broad wavelengths, mediated through multiple photoreceptors, and requires inactivation of COP1 and PIF photomorphogenesis inhibitors. Such induced *ATH1* prevents elongation of rosette internodes by maintaining the rib zone area of the SAM in an inactive state. In the absence of light, Arabidopsis plants cannot complete seedling establishment after germination due to inactivity of the shoot apical meristem (SAM). Light requirement for SAM activation can be overcome by availability to the meristem of metabolizable sugars, such as sucrose. However, under these conditions plants fail to establish a typical compact rosette and display a caulescent growth habit. We show that this is due to insufficient expression of *ATH1* at the SAM. ATH1 induction restores rosette habit in dark-grown plants through inhibition of *PIF* gene expression. Together, this

suggests that a SAM-specific, double-negative ATH1-PIF feedback loop is at the basis of Arabidopsis rosette habit. Induction of *ATH1* expression and restoration of rosette habit in darkness also occurs at increased levels of sucrose. Both sugar and light signals that induce *ATH1* are mediated by TOR kinase. Overall, these results support a fundamental role for ATH1 in Arabidopsis rosette habit and further strengthen a role for TOR kinase as a central hub for integration of energy and light signals controlling organogenesis at the SAM.

Key words: *ARABIDOPSIS THALIANA* HOMEOBOX 1 (ATH1), rosette growth habit, photomorphogenesis, TOR kinase, meristem activity

Introduction

Plants, as sessile organisms, are equipped with sophisticated mechanisms to sense the environment and to adapt their growth and development accordingly. Being photoautotrophs, plants are especially attuned to the light environment. This is well illustrated by the dramatic differences in appearance between light- and dark-grown seedlings. In Arabidopsis, dark-grown seedlings have a typical etiolated phenotype, characterized by an elongated hypocotyl, formation of an apical hook, closed and unexpanded cotyledons, and an arrested shoot apical meristem (SAM). Exposure of seedlings to light results in inhibition of hypocotyl elongation, opening of the apical hook, opening and expansion of cotyledons, and SAM activation (Chen and Chory, 2011; Arsovski et al., 2012; Pfeiffer et al., 2016; Mohammed et al., 2017; Janocha et al., 2021). The active SAM gives rise to the aerial portion of the plant via the formation of organ primordia at its flanks. During the vegetative growth phase, leaf primordia arise in a spiral phyllotaxy to form a compact, basal rosette in which internode elongation remains arrested. In the absence of light, SAM activity can be induced by exposing the SAM to metabolizable sugar, such as sucrose, glucose, or fructose (Araki and Komeda, 1993; Roldán et al., 1999). Both light- and sugar-mediated SAM activation involve TARGET OF RAPAMYCIN (TOR) kinase, a central component in energy sensing, such that it promotes SAM activity in favorable conditions (Pfeiffer et al., 2016; Li et al., 2017; Mohammed et al., 2017; Janocha et al., 2021). It has been proposed that light, via photoreceptor signaling through CONSTITUTIVE PHOTOMORPHOGENIC1 (COP1), plays a permissive role toward energy signaling in the SAM, possibly by controlling sugar import into the meristem

(Mohammed et al., 2017). This might explain why direct access of the SAM to metabolizable sugar can activate the meristem in the absence of light.

Sugar-induced dark morphogenesis of Arabidopsis plants follows the same developmental phases as light-grown plants. However, in sugar-induced, dark-grown plants stem elongation is not inhibited during vegetative development contrary to light-grown plants. Consequently, such dark-grown plants no longer display a rosette habit and elongated internodes are present between adjacent 'rosette' leaves (Roldán et al., 1999; Mohammed et al., 2017). A similar loss of rosette habit has been observed in light-grown Arabidopsis plants lacking functional phytochrome (phy) and/or cryptochrome (CRY) photoreceptors. Control of rosette internode elongation in response to a low red to far-red (R:FR) ratio of light or end-of-day FR light (EOD-FR) is mediated by phyA, phyB, phyD, and phyE in a functionally redundant manner (Devlin et al., 1996; Whitelam and Devlin, 1997; Devlin et al., 1998; Whitelam et al., 1998; Devlin et al., 1999; Roldán et al., 1999; Mazzella et al., 2000; Devlin et al., 2003; Franklin et al., 2003a). In addition, ambient temperature has been reported to modulate the light-regulation of Arabidopsis rosette habit. At elevated ambient temperature, phyB and CRY1 redundantly suppress internode elongation during vegetative development (Mazzella et al., 2000). A compact rosette habit thus is a *bona fide* photomorphogenic trait in Arabidopsis. However, despite numerous observations and the economic importance of rosette habit in vegetable crops, this aspect of photomorphogenic development has been paid little attention and molecular events involved downstream of photoreceptor signaling remain to be identified.

In Arabidopsis, internode elongation reflects the activity of the basal part of the SAM, the rib zone. In light-grown plants, the rib zone is compact and mitotically inactive during vegetative growth, resulting in the formation of a compact rosette. At floral transition, the rib zone becomes activated to provide cells for rapid elongation of the internodes of the inflorescence stem (Vaughan, 1955; Sachs et al., 1959; Peterson and Yeung, 1972; Jacqmard et al., 2003; Bencivenga et al., 2016; Serrano-Mislata et al., 2017). Previously, ectopic expression of the Three-Amino Acid Loop Extension (TALE) homeobox gene *ARABIDOPSIS THALIANA HOMEOBOX GENE1* (*ATH1*) was shown to suppress growth of the inflorescence stem, due primarily to inhibition of internode elongation (Cole et al., 2006; Gómez-Mena and Sablowski, 2008; Rutjens et al., 2009; Ejaz et al., 2021). In wild-type plants, *ATH1* is expressed in the vegetative SAM, and its expression in this tissue is rapidly downregulated at floral transition, when stem growth is initiated. In addition, in

plants lacking functional ATH1, the subapical region, where the rib zone is located, is enlarged during vegetative development, suggesting that ATH1 restricts growth of this part of the SAM (Proveniers et al., 2007; Gómez-Mena and Sablowski, 2008). In line with this, light-grown *ath1* mutants display slightly elongated rosette internodes, resembling those of higher-order photoreceptor mutants (Li et al., 2012; Ejaz et al., 2021). *ATH1* was originally identified in a screen for light-regulated transcription factor genes and its expression is induced by light during seedling de-etiolation (Quaedvlieg et al., 1995). In dark-grown seedlings of the photomorphogenic *cop1* mutant *ATH1* mRNA levels are elevated as well, suggesting that *ATH1* expression is under the control of COP1, a negative regulator of photomorphogenesis (Quaedvlieg et al., 1995; Proveniers et al., 2007). In line with this, *cop1* loss-of-function mutants exhibit a constitutive deetiolated phenotype in darkness, including formation of a compact rosette (Deng and Quail, 1992). Together with SUPPRESSOR OF PHYA-105 (SPA) proteins, COP1 forms an E3 ubiquitin ligase complex, which acts by regulating the stability of photomorphogenesis-promoting transcription factors. In addition, COP1/SPA stabilizes proteins of the PHYTOCHROME INTERACTING FACTOR (PIF) family in darkness to promote etiolation (Ponnu and Hoecker, 2021)). Upon exposure to light, phytochromes physically interact with PIF proteins and promote their turnover, resulting in de-etiolation (Pham et al., 2018a; Ponnu and Hoecker, 2021).

Here we show that ATH1 confers rosette habit in light-grown, vegetative Arabidopsis plants by integration of signals from multiple photoreceptors. In wildtype plants, *ATH1* expression can be induced by blue, red, and far-red light and this requires both the PHY and CRY families of photoreceptors. Dark-grown wildtype plants and higher-order photoreceptor mutants display strongly reduced levels of *ATH1* in the SAM and transgene expression of *ATH1* is sufficient to restore rosette habit in both cases. Finally, we introduce a regulatory feedback loop whereby multiple PIFs (i.e., PIF1, PIF3, PIF4, and PIF5) and ATH1 repress each other's expression in a tissue-specific manner, contributing to the maintenance of rosette habit.

Furthermore, in the absence of light, *ATH1* expression can be induced by the direct availability of metabolic sugars to the SAM. We show that increasing amounts of sucrose result in a corresponding increase of *ATH1* expression and associated increased inhibition of vegetative internode elongation. Our data further show that both light- and metabolic signal-mediated induction of *ATH1* at the SAM requires activation of TOR kinase.

Results

Induction of *ATH1* expression restores a compact rosette habit in dark-grown seedlings

In higher plants, most of the above-ground part is generated by a combination of cell division, cell growth, cell expansion, morphogenesis, and differentiation at or near the SAM. Upon germination, the SAM becomes rapidly activated by light and starts a highly coordinated cell division program that continues throughout vegetative growth. In contrast, stem cells remain dormant when Arabidopsis plants are germinated and grown in darkness (Pfeiffer et al., 2016; Mohammed et al., 2017) As a result, dark-grown seedlings display a typical etiolated phenotype. This morphogenetic arrest can be overcome by the availability of sucrose to the aerial part of the plant. Sugar-induced dark morphogenesis of Arabidopsis plants follows the same developmental phases as light-grown plants. However, such plants fail to develop a compact rosette (Figure 1A, B) (Roldán et al., 1999; Mohammed et al., 2017).

The compact rosette habit of light-grown Arabidopsis plants is conferred by ATH1 (Li et al., 2012; Ejaz et al., 2021). We tested whether *ATH1* expression is sufficient for development of a compact rosette in dark-grown plants. For this a fusion protein of ATH1 with the rat glucocorticoid receptor hormone-binding domain (HBD) under the control of the CaMV 35S promoter (*35Spro:ATH1-HBD*; Rutjens et al., 2009) was expressed in plants grown in continuous darkness in the presence of one percent sucrose (Figure 1A, B). Induction of nuclear expression of ATH1 using dexamethasone (Dex) resulted in strong repression of rosette internode elongation and, consequently, restoration of rosette habit in dark-grown plants, while Col-8 control plants and mock-treated *35Spro:ATH1-HBD* plants displayed elongated vegetative internodes, resulting in loss of rosette habit (Figure 1A, B). Surprisingly, in darkness in the presence of sucrose vegetative internodes of loss-of-function *ath1* mutants (Proveniers et al., 2007), were slightly more elongated than those in Col-8 wild-type control plants (Figure 1A, B), suggesting that *ATH1* might still be expressed to some extend in the absence of light, despite previous research indicating the absence of *ATH1* expression in dark-grown plants (Quaedvlieg et al., 1995).

Possibly, the addition of one percent sucrose to the growth medium, necessary to induce dark morphogenesis, results in induction of *ATH1* gene expression in the absence of light. To investigate whether *ATH1* is expressed in dark-grown seedlings in the presence of sucrose, we compared *ATH1* expression between light- and dark-grown seedlings, both supplied with one percent exogenous sucrose. As can be seen in Figure 1C, *ATH1* expression is significantly

decreased but not entirely abolished in dark-grown seedlings. Compared to a light-grown situation, *ATH1* expression is more than 80% reduced (Figure 1D). Furthermore, in accordance with Quaedvlieg *et al.* (1995), *ATH1pro:GUS* analysis showed no *ATH1* induction in dark-grown plants in absence of sucrose, whereas *ATH1* promoter activity could be gradually induced by addition of increasing amounts of sucrose to the growth medium (Figure 1E). These findings indicate a dose-dependent relationship between sucrose concentration and ATH1 expression in dark-grown plants. Thus, in dark-grown Arabidopsis plants, sucrose can substitute for light to induce *ATH1* expression at the shoot apex.

Importantly, these observations suggest a close correlation between the amount of *ATH1* expressed at the shoot apex and the extent to which rosette internode elongation is suppressed. To test this, we analyzed elongation of vegetative internodes in dark-grown *35Spro:ATH1-HBD* plants exposed to increasing concentrations of Dex (Figure 1F). As Dex promotes nuclear accumulation of ATH1, increased Dex concentrations are expected to result in increased levels of nuclear ATH1 and, hence, stronger inhibition of internode elongation. This is exactly what was observed, with a maximum inhibitory effect on internode elongation in plants exposed to a Dex concentration of 100 nM, whereas none of the Dex concentrations tested had any effect on rosette internode elongation in control plants (Figure 1F). In line with these results, dark-grown Col-8 plants displayed increasing inhibition of rosette internode elongation when exposed to increasing concentrations of sucrose (0.5, 1.0, 1.5, or 2.5%). In these seedlings, rosette habit was completely restored in the presence of 2.5% sucrose, comparable to fully-induced dark-grown *35Spro:ATH1-HBD* plants (Figure 1A, F, G). As expected, in *ath1-4* mutant plants, internode elongation remained unaffected at all sucrose concentrations tested (Figure 1G). Taken together, this strongly suggests that sucrose-induced repression of rosette internode elongation in dark-grown plants is *ATH1*-dependent. These findings further show that typical loss of rosette habit, generally observed in sucrose-stimulated, dark-grown Arabidopsis plants, can be attributed to suboptimal *ATH1* expression at the shoot apex.

SAM morphology of sucrose-stimulated, dark-grown seedlings strongly resembles that of light-grown *ath1* mutants

In light-grown *ath1* mutants elongation of vegetative internodes results from activation of stem development, as reflected by premature rib zone (RZ) activity (Roldán et al., 1999; Rutjens et al.,

2009; Ejaz et al., 2021). To confirm that the elongated internode phenotype observed in dark-grown Arabidopsis plants also results from premature activation of stem development, we imaged shoot apices of both light- and dark-grown Col-8 seedlings and compared these with those of light-grown *ath1-4* seedlings (Figure 2A-C). We then measured the lengths of individual cells that make up a central cell file running from the L1 layer into the subapical RZ region of the SAM until where the hypocotyl vascular strands converge (Figure 2F). As expected, when grown for five days in continuous light, *ath1-4* mutants displayed elongated vegetative internodes, whereas those of Col-8 plants remained compact (Figure S2A, C). Comparing the *ath1-4* and Col-8 genotypes showed the first four cells of the central cell file to be of similar length. In contrast, more basal cells, in the RZ region, were significantly more elongated in *ath1-4* mutants (Figure 2A, C, F). This is in line with previous observations by Rutjens et al. (2009) who found that in *ath1* mutants RZ cells are more longitudinally elongated than in wild-type control plants. A similar SAM morphology was observed in Col-8 seedlings grown in darkness and supplied with one percent sucrose. Under these conditions, Col-8 rosette habit is no longer maintained, similar to light-grown *ath1* mutants, (Figure S2B). Compared to light-grown Col-8 seedlings, basal cells were significantly more elongated in dark-grown Col-8 seedlings in the presence of sucrose, whereas the lengths of the four apical central cells of light-grown Col-8 seedlings were not statistically different compared to dark-grown Col-8 (Figure 2A-C, F). Morphologically these basal cells resemble the elongated RZ cells of *ath1-4* mutants (Figure 2B, C).

Since ectopic expression of *ATH1* restored a compact rosette habit in dark-grown seedlings (Figure 1A, B; S2D, E), we examined whether this is caused by inhibition of RZ activity. While dark-grown mock-treated *35Spro:ATH1-HBD* plants showed a SAM morphology similar to that of dark-grown Col-8 control plants, induction of *ATH1* specifically repressed cell elongation in the basal RZ cells (Figure 2B, D-F). Taken together, these findings indicate that loss of rosette habit in Arabidopsis plants in the absence of light, results from premature RZ activation due to significantly reduced *ATH1* expression at the shoot apex. Moreover, we noted that in dark-grown seedlings the central cell file always contained more cells than that of light grown plants (Figure 2A-F). This seems to be an effect of light independent of ATH1 as this was found for all genotypes analyzed.

ATH1 functions downstream of multiple photoreceptors to maintain a compact rosette habit

Loss of rosette habit due to elongation of vegetative internodes, reminiscent of the caulescent growth habit of sucrose-induced, dark-grown Arabidopsis plants, can also be observed in light-grown photoreceptor mutants. Elongation of vegetative internodes is clearly visible in higher order mutants, such as *phyA phyB* (*phyAB*), *phyA phyB phyD* (*phyABD*), *phyA phyB phyE* (*phyABE*), *phyB phyD phyE* (*phyBDE*), *phyA phyB phyD phyE* (*phyABDE*) mutants, a quintuple *phy* mutant, and *phyB cry1* mutants (Devlin et al., 1996; Devlin et al., 1998; Whitelam et al., 1998; Devlin et al., 1999; Mazzella et al., 2000; Devlin et al., 2003; Strasser et al., 2010; Li et al., 2012). *ATH1* expression is strongly light-dependent (Quaedvlieg et al., 1995; Roldán et al., 1999; Proveniers et al., 2007) (Figure 1C, D), raising the question of whether light-mediated expression of *ATH1* depends on these photoreceptors. If so, it is of interest to investigate whether reduced levels of *ATH1* can explain the significant elongation of internodes between adjacent rosette leaves displayed by the respective photoreceptor mutants. To answer these questions, we first grew wild-type seedlings under different wavelengths of light and analyzed *ATH1* mRNA levels (Figure 3A). This revealed that apart from white light, as reported before, monochromatic blue, red, and far-red light induce *ATH1* expression to significant levels, suggesting that *ATH1* is under control of multiple photoreceptors.

We next determined *ATH1* promoter activity and mRNA levels in a series of phytochrome and/or cryptochrome photoreceptor mutants grown under various light quality conditions (Figure 3C; S1). Whereas *ATH1* transcript levels in response to white light were somewhat decreased in *phyB* and *cry1* single mutants, combination of both mutations significantly affected white light-mediated induction of *ATH1* expression (Figure 3C; S1). Similarly, introduction of additional *phy* mutations in a *phyB* background or the combination of the phytochrome chromophore biosynthesis mutant *hy1* with *cry1* and/or *cry2* mutations resulted in moderate to severe reduction in *ATH1* transcript levels in white light, confirming that light-mediated regulation of *ATH1* is under control of multiple photoreceptors (Figure 3C, S1A). Repeating experiments under monochromatic red, far-red, or blue-light conditions revealed that red-light-mediated induction of *ATH1* expression is mostly the result of phyB function, in cooperation with phyD and phyE (Figure 3C, S1B), whereas phyA is largely responsible for *ATH1* induction in far-red light (Figure 3C, S1D). Under monochromatic blue light, CRY1 and CRY2 redundantly contribute to *ATH1* gene activity, with CRY1 being the predominant cryptochrome under the conditions tested (Figure 3C, S1C). We further noticed that all photoreceptor mutants previously reported to have a loss of rosette habit,

248 including *phyBDE* and *phyB cry1* mutants (Mazzella et al., 2000; Li et al., 2012), all had severely
249 reduced levels of *ATH1* (Figure 3C). Internode elongation reflects activity of the basal part of the
250 SAM, the rib zone, and ATH1 controls activity of this tissue. We compared the spatial activity of
251 the *ATH1* promoter in these higher order photoreceptor mutants with that in L*er* control plants and
252 a *phyB* mutant. In line with previous observations (Proveniers et al., 2007), high levels of GUS
253 activity were present in the SAM and emerging leaf primordia of L*er ATH1pro:GUS* seedlings
254 grown in white light. Corroborating our qPCR data, GUS activity was significantly reduced in
255 *phyB cry1 ATH1pro:GUS* and *phyBDE ATH1pro:GUS* plants, whereas in a *phyB* background GUS
256 activity was only moderately affected (Figure 3B). Interestingly, the largest effect of reduced
257 photoreceptor signaling on *ATH1* promoter activity was in the SAM region. In both *phyB cry1* and
258 *phyBDE* backgrounds hardly any residual GUS activity could be detected in the SAM, including
259 the rib zone area, whereas in leaf primordia a more modest reduction in *GUS* expression was
260 observed (Figure 3B). Taken together, these findings suggest that phytochrome and cryptochrome
261 photoreceptor families contribute to rosette growth habit in light-grown vegetative Arabidopsis
262 plants through induction of *ATH1* expression in the SAM.
263 To further test this hypothesis, we constitutively expressed *ATH1* (*Pro35S:HA-ATH1*) in a number
264 of photoreceptor mutants that display elongation of vegetative internodes when grown under
265 standard, long-day conditions, with partial to complete loss of rosette growth habit as a result
266 (Figure 3D, E). Under these growth conditions, L*er* control plants never display any detectable
267 elongation of rosette internodes. In contrast, internodes of *phyB*, *phyBcry1*, *hy1cry1*, and
268 *hy1cry1cry2* mutants were visibly elongated (Figure 3D, E). Strikingly, the extent to which rosette
269 internode elongation was affected in these genotypes nicely correlates with earlier observed *ATH1*
270 expression levels in the respective mutant backgrounds (Figure 3C-E; S1A). As expected,
271 constitutive expression of *ATH1* completely suppressed elongation of vegetative internodes in all
272 four mutants analyzed (Figure 3D, E). Thus, reestablishing high levels of *ATH1* expression is
273 sufficient to restore a compact rosette habit in higher order photoreceptor mutants.
274 In conclusion, rosette growth habit, quintessential for light-grown vegetative Arabidopsis plants,
275 is imposed by *ATH1* activity in the shoot apex under control of multiple blue and red/far-red light
276 photoreceptors.
277

Light-mediated regulation of *ATH1* expression is controlled by central light signaling components

ATH1 was first identified in our lab as a light-regulated transcription factor gene that is derepressed in dark-grown *cop1* mutants (Quaedvlieg et al., 1995). COP1, in conjunction with SPA proteins, functions as a repressor of light signaling in darkness. In the light, phytochrome family members, activated by red or far-red light (in case of phyA) wavelengths, and cryptochromes 1 and 2, activated by blue light wavelengths, suppress the activity of the COP1/SPA complex to promote photomorphogenesis (Ponnu and Hoecker, 2021). Light-mediated *ATH1* expression can be induced by all three light qualities, involving both phytochrome and cryptochrome family members. Since COP1 is a downstream signaling component of these photoreceptor families, we analyzed the role of COP1 in the regulation of *ATH1* expression and rosette growth habit. First, we compared *ATH1* expression levels in dark-grown Col-8 seedlings to those in dark-grown *cop1-4* mutants, both in the presence and absence of sucrose (Figure 4A). As shown before, in Col-8 *ATH1* expression can be induced in darkness by the addition of sucrose to the growth medium to a final concentration of one percent, whereas in the absence of sucrose transcript levels remain low. In line with the observations by Quaedvlieg et al. (1995), in dark-grown *cop1-4* mutants, carrying a mild loss-of-function allele of *COP1*, *ATH1* expression was clearly derepressed. Already in the absence of sucrose, *ATH1* mRNA levels accumulated to levels higher than those observed in Col-8 control plants supplied with one percent sucrose. In the presence of sucrose, *cop1-4 ATH1* transcript levels increased even further (Figure 4A), indicating that light and sucrose signaling contribute, at least partially, independently to induce of *ATH1* gene expression.

Consistent with these observations, vegetative internodes of dark-grown *cop1-4* mutants supplemented with one percent sucrose failed to elongate, contrasting to those of Col-8 control plants. As a result, *cop1-4* plants adopted a compact rosette growth habit, reminiscent of that seen in dark-grown, induced *35Spro:ATH1-HBD* plants supplemented with sucrose (Figure 4B, C; 1B). The compact rosette habit in darkness is lost in *cop1-4 ath1-4* double mutants, indicating that this photomorphogenesis phenotype requires ATH1 activity (Figure 4C). However, when compared to *ath1-4* single mutants, vegetative internode elongation in *cop1 ath1* double mutants is much reduced, suggesting the involvement of other loci apart from *ATH1* (Figure 4B, C). In the absence of sucrose, both Col-8 and *cop1-4* seedlings failed to develop beyond the seedling stage in the dark

(Figure 4C), most likely due to the lack of stem cell activation at the shoot apex (Pfeiffer et al., 2016).

In addition to COP1, PIFs also function downstream of both phytochrome and cryptochrome light signaling (Ma et al., 2016; Pedmale et al., 2016; Pham et al., 2018b). PIF-family transcription factor proteins function as negative regulators of light responses, in a partially redundant manner, to maintain skotomorphogenesis in dark-grown seedlings. Upon exposure to light, phytochromes promote the turnover of PIFs, whereas photoactivated CRY1 has been shown to interact with PIF4, resulting in suppression of the transcriptional activity of PIF4 (Ma et al., 2016). As a consequence, plants switch from skotomorphogenesis to photomorphogenesis. In line with this, the quadruple *pif1pif3pif4pif5* (*pifq*) mutant displays a constitutively photomorphogenic phenotype in darkness (Leivar et al., 2009). In addition to their role as transcription factor proteins, PIFs can directly interact with COP1, thereby enhancing substrate recognition and ubiquitination activity of the COP1 E3 ligase complex (Xu et al., 2014; Kathare et al., 2020). Therefore, we tested whether PIF family members act as upstream mediators of *ATH1* gene expression in the regulation of rosette habit in Arabidopsis. To this end, we first analyzed rosette habit in a series of dark-grown single, double, triple, and quadruple *pif* mutant combinations in the presence of one percent sucrose. Under these conditions, Col-8 control plants display a clearly visible elongation of vegetative internodes, resulting in loss of rosette habit. In contrast, in the quadruple *pifq* mutant complete repression of rosette internode elongation was observed, resulting in the formation of a compact rosette in the absence of light (Figure 5A). Of the single *pif* mutants tested, only *pif4* displayed a significant reduction in rosette internode length (37% less elongation) when compared to control plants, whereas *pif3* and *pif7* mutants were largely unaffected. None of the double (*pif1pif3*, *pif3pif4*, *pif4pif5*) or triple mutants (*pif1pif3pif4*, *pif1pif3pif5*, *pif3pif4pif5*) were as compact as the *pifq* mutant (Figure 5A), indicating that PIF1, PIF3, PIF4, and PIF5 redundantly contribute to elongation of rosette internodes in etiolated plants. Of these four proteins, PIF4 contributes the most, as can be inferred from its single mutant phenotype and the significant inhibition of internode elongation in all higher order mutants carrying a *pif4* allele, while inhibition of internode elongation is absent in *pif1pif3* mutants and only subtly enhanced by *pif5* in *pif4pif5* and *pif3pif4pif5* mutants (Figure 5A).

The prominent role of PIFs in the suppression of photomorphogenesis and the striking resemblance of *pifq* mutants to DEX-induced *35Spro:ATH1-HBD* plants when grown in darkness (Figure 1A,

B), prompted us to investigate whether PIF proteins are upstream regulators of *ATH1*. ATH1 functions in the shoot apex to control internode elongation. Therefore, *ATH1* transcript levels were compared between shoot apices of 14-day-old, dark-grown Col-8, *pif4* and *pifq* plants (Figure 5B). A significant increase in *ATH1* mRNA levels was observed in both *pif4* (1.7x higher) and *pifq* (3x higher) mutants when compared to control plants, in line with the observed effects on inhibition of internode elongation. To examine whether this increase in *ATH1* expression is responsible for the formation of the compact rosette habit observed in *pifq* mutants when grown in darkness, we introduced the *ath1-3* loss-of-function allele in the *pifq* mutant background and tested the resulting plants for rosette internode elongation when grown in darkness in the presence of one percent sucrose (Figure 5C). Under these conditions *pifq* mutants grow a compact rosette, whereas rosette habit is lost in Col-8 control plants and *ath1* mutants, with the latter having the most elongated internodes (Figure 5A, C). Surprisingly, vegetative internodes of *pifq ath1* plants were only mildly elongated, resulting in a partial loss of rosette habit. Compared to *ath1* plants, internodes of *pifq ath1* were on average 70% shorter (Figure 5C). This unexpected result suggests that PIFs control rosette internode elongation mostly independent of ATH1 or that the relationship between PIFs and ATH1 is more complex. Recently, PIF4 has been identified as a direct binding target of ATH1 (Ejaz et al., 2021). In this study no significant differences in *PIF4* expression could be detected between *ath1* and WT plants when analyzed on a whole-seedling basis. However, this does not rule out the presence of a regulatory feedback loop between PIFs and ATH1 at a tissue-specific level. Such ATH1-PIFs feedback regulation could explain the observed internode phenotype in *pifq ath1* mutants. To explore the presence of such regulatory interaction between ATH1 and PIFs, we quantified expression of PIF family genes in genotypes with altered expression of *ATH1*. We specifically focused on PIF gene expression in shoot apices (Figure 5D, E) as ATH1 activity in the shoot apex underlies its inhibitory effect on internode elongation and PIFs are ubiquitously expressed (Wu et al., 2020) In sucrose-supplied, dark-grown plants *ATH1* expression levels are low (Figure 1C, D) and ATH1 is expected to have an inhibitory effect on *PIF* expression. Therefore, inducible *35Spro:ATH1-HBD* plants were used to examine the effect of ATH1 on *PIF1*, *PIF3*, *PIF4* and *PIF5* mRNA levels in dark conditions (Figure 5D). In light-grown vegetative plants, *ATH1* expression levels at the shoot apex are relatively high. Therefore, in light conditions the effect of ATH1 on gene expression of these four *PIFs* was analyzed using *ath1-3* plants (Figure 5E). In both conditions, a clear effect of ATH1 on *PIF* gene expression was observed. In dark-

grown plants, induction of ATH1 accumulation in the nucleus resulted in significant down-regulation of *PIF1*, *PIF3* and *PIF4*, and, to a lesser extent, *PIF5* expression (Figure 5D). On the other hand, in light-grown plants mRNA levels of *PIF1*, *PIF3*, *PIF4*, and *PIF5* were up-regulated in the absence of *ATH1*. In *ath1* plants, PIF1 levels in the shoot apex were up to 9 times higher when compared to control plants, whereas *PIF3*, *PIF4*, and *PIF5* levels were 2.5-3 times increased (Figure 5E). When analyzed on a whole-plant level, under both conditions no significant differences in *PIF* expression levels could be detected between either *35Spro:ATH1-HBD* or *ath1-3* plants and control plants (data not shown). Together, these results indicate that ATH1 acts as a negative regulator of, at least, *PIF1*, *PIF3*, *PIF4*, and *PIF5* gene expression, in a tissue-specific manner. These data support the presence of a regulatory feedback loop at the transcriptional level between ATH1 and PIF family members where ATH1 and PIFs repress each other's expression. This ATH1-PIF interdependence for suppression of rosette internode elongation could explain the partial loss of rosette habit in *cop1-4 ath1-4* double mutants observed earlier (Figure 4B, C), since functional PIF1, PIF3, PIF4 and PIF5 proteins are required for dark-mediated rosette internode elongation in the absence of ATH1 (Figure 5C) and these PIF proteins are degraded in darkness in the presence of a *cop1-4* mutation (Pham et al., 2018c; Pham et al., 2018a).

Overall our data show that loss of rosette habit in dark-grown Arabidopsis plants is part of a skotomorphogenic developmental program, achieved through active repression of *ATH1* gene expression, mediated by COP1 and PIF family members.

Photosynthetic sugars are not a prerequisite for light-induced *ATH1* expression

ATH1 expression in the shoot apex can be induced both by light and sucrose (Figure 1D, E; 3A). Since light not only acts as a developmental signal, but also as an energy source through photosynthesis, we wondered about the exact role of light in the induction of *ATH1* gene expression. Therefore, we examined *ATH1* promoter activity in plants where photosynthesis was chemically inhibited. To this end, *ATH1pro:GUS* seedlings were grown in darkness for five days, without metabolizable sugar in the medium to deplete plant metabolizable sugar. Five hours before light treatment, either norflurazon or lincomycin repressors of photosynthesis were added to the medium, after which plants were grown for an extra two days in continuous light (Figure 6A). Compared to mock treatment (0.1% ethanol), inhibition of photosynthesis by chemical interference resulted in slightly reduced *ATH1* expression (Figure 6B). To avoid potential indirect effects of

these pharmacological treatments, we also examined the impact of CO_2 withdrawal on *ATH1* expression. Removal of CO_2 from the atmosphere, through chemical absorption by NaOH + CaO, inhibits photosynthetic carbon assimilation and, thereby, the accumulation of metabolizable sugars. Similar to the pharmacological treatments in the absence of photosynthesis, *ATH1* promoter activity was decreased, but GUS staining was still clearly visible (Figure 6B; S3A). This indicates that *ATH1* gene expression is affected by light acting both as a developmental trigger and as a source of metabolizable sugars through photosynthesis. It further shows that sucrose produced through photosynthesis contributes to, but is not a prerequisite for light-induced *ATH1* expression. This is in line with the observation that *ATH1* expression is derepressed in dark-grown *cop1* seedlings even in the absence of sucrose (Figure 4A).

Sugars function as energy resource and as signaling molecules (Li and Sheen, 2016). To distinguish between these two functions in the induction of *ATH1* expression at the SAM Col-8 plants were grown in darkness in the presence of either sorbitol, sucrose, glucose, fructose, or palatinose, followed by quantification of *ATH1* mRNA levels and promoter activity (Figure 6C; S3C). Sorbitol and palatinose are both non-metabolizable sugars. Palatinose is a metabolically inactive structural isomer of sucrose that was shown to function as a signaling molecule, whereas sorbitol is neither metabolized nor a signaling molecule (Ramon et al., 2008). Glucose, fructose and sucrose are metabolizable sugars also known to function as signaling molecules (Rabot et al., 2012). Neither sorbitol nor palatinose addition resulted in a significant induction of *ATH1* expression, whereas a clear increase in *ATH1* could be observed when either sucrose, glucose or, to a lower extent, fructose was present in the growth medium (Figure 6C). These findings strongly suggest that sugars as energy source induce *ATH1* expression.

Sucrose and light independently regulate *ATH1* expression via TOR kinase

TOR kinase, a critical sensor of resource availability, is required for the activation of both shoot and root apical meristems (Xiong et al., 2013; Pfeiffer et al., 2016; Li et al., 2017). TOR kinase integrates, among others, energy and environmental cues, including light signals to direct growth and development. The fundamental role of TOR kinase in coordinating growth and development downstream of light and energy signals, led us to investigate whether induction of *ATH1* expression involves TOR kinase activity. Employing a similar experimental setup as mentioned in the previous section, the effect of the ATP-competitive TOR kinase inhibitor AZD-8055 on light-

and sucrose-induced *ATH1* promoter activity was studied. AZD-8055 was added to 5-day-old, dark-grown *ATH1pro:GUS* seedlings. After 5 hours either sucrose was added to the growth medium and plants were left to continue growing in darkness, or plants were shifted to continuous light conditions for 48 hours (Figure 6A). Light-mediated induction of *ATH1* promoter activity was efficiently suppressed by AZD-8055, resulting in complete inhibition of promoter activity at a concentration 0.5 µM (Figure 6D). Similarly, addition of AZD-8055 fully inhibited the positive effect of sucrose on ATH1 promoter activity at the shoot apex (Figure 6E; S3B).

AZD-8055 is a selective and potent TOR inhibitor (Montané and Menand, 2013; Dong et al., 2015), but the use of pharmacological agents poses a risk of non-anticipated side effects. Loss-of-function *tor* mutants are embryo lethal (Menand et al., 2002), and therefore the previously reported ethanol-inducible TOR-RNAi line, *35S:ALCR alcA:RNAi-TOR* and its control line *35S:ALCR alcA:GUS* (Deprost et al., 2007), were used to further study the effects of reduced TOR kinase activity on *ATH1* gene expression. In line with our AZD-8055 experiments, conditional silencing of the AtTOR gene by ethanol in *35S:ALCR alcA:RNAi-TOR* seedlings led to complete inhibition of sucrose-mediated induction of *ATH1* expression (Figure 6F). These results imply that light and metabolic signals converge on TOR kinase in controlling induction of *ATH1* expression at the SAM.

Recently, it was reported that TOR kinase and downstream signaling contribute to the de-etiolation process and that COP1 represses TOR activity during skotomorphogenic development (Chen et al., 2018). We therefore tested whether derepression of *ATH1* expression in dark-grown *cop1* mutants is also TOR dependent. QPCR analysis revealed that this is indeed the case, as in the presence of AZD-8055 *ATH1* expression is no longer derepressed in dark-grown *cop1-4* plants (Figure S4).

In conclusion, these findings suggest TOR kinase integrates light and sucrose signals leading to activation of *ATH1* gene expression at the shoot apex (Figure 7). Upstream of TOR kinase, a PHY-COP1 regulatory pathway functions as a negative regulator of TOR activity. When grown in darkness, COP1 inhibits TOR, resulting in repression of *ATH1*. As a consequence, in dark-grown plants compact rosette habit is lost due to activation of stem development, resulting in the elongation of vegetative internodes. In the light, COP1 activity is inhibited allowing for TOR kinase to induce *ATH1* expression in the shoot apex as part of the deetiolation process, giving rise to the compact rosette habit that is characteristic for *A. thaliana*.

Discussion

In plants most of the adult body is formed post-embryonically by the continuous activity of pools of undifferentiated progenitor cells: the shoot and root apical meristems. Both apical meristems are established during plant embryogenesis. At the completion of embryogenesis the apical meristems are quiescent, but become reactivated after seed germination. In *A. thaliana* (Arabidopsis), light is crucial for reactivation of the shoot apical meristem (López-Juez et al., 2008; Arsovski et al., 2012; Pfeiffer et al., 2016; Mohammed et al., 2017). A direct outcome of light-activation of the meristem is the production of leaves. In rosette plants, such as Arabidopsis, the newly formed leaves give rise to a basal rosette: a whorl of leaves that has little to no elongation between successive nodes. The rosette habit is widespread amongst flowering plants and provides several advantages compared to taller, less compact plants, such as protection from (a)biotic stresses (Schaffer and Schaffer, 1979; Bello et al., 2005; Larcher et al., 2010; Thomson et al., 2011; Fujita and Koda, 2015). In Arabidopsis, light requirement for SAM activation can be overcome by availability of metabolizable sugars, such as sucrose, to the meristem (Roldán et al., 1999; Li et al., 2012). However, under such conditions plants fail to establish a typical compact rosette. Instead, they display a caulescent growth habit due to elongation of rosette internodes. Here we show that this dramatic change in growth habit in the absence of light is caused by premature activation of the rib zone due to insufficient expression of the light-mediated TALE homeobox gene *ATH1* in the shoot meristem. Our observations confirm a fundamental role for ATH1 in Arabidopsis rosette growth habit and supports a role for TOR kinase as a central hub for integration of energy and light signaling in controlling cell differentiation and organ initiation at the SAM.

Previously, both activation of the SAM following germination, via induction of *WUSCHEL* (*WUS*), as well as subsequent initiation of leaf primordia were shown to be synergistically controlled by light-signaling pathways and photosynthesis-derived sugars, both conveyed by TOR kinase (Li et al., 2012; Pfeiffer et al., 2016). Here we show that induction of *ATH1* expression at the SAM, required to inhibit rib zone activation during vegetative development, is additively induced by sugar and light-signaling and that TOR kinase activity is essential for both inputs. Thus, TOR kinase integrates light and energy signals to activate the central population of stem cells in the SAM and subsequent differentiation processes at the periphery of the meristem but, interestingly, also represses differentiation processes by inhibiting rib zone activity at the basal

494 part of the meristem. Induction of *ATH1* through these signals might indirectly result from SAM
495 activation. However, we think this is unlikely as, in the absence of sucrose, the SAM of dark-
496 grown *cop1* mutants remains dormant, while *ATH1* is expressed to relatively high levels. In
497 addition, SAM activation and *ATH1* induction responses differ in their sensitivity to sucrose.
498 Sucrose concentrations adequate to activate the SAM and initiate organogenesis, fail to induce
499 significant levels of *ATH1*.
500 How TOR kinase controls *ATH1* promoter activity is currently unknown. TOR kinase is a major
501 regulator of mRNA translation in all eukaryotic cells (Schepetilnikov and Ryabova, 2017).
502 Moreover, light/dark transitions are also known to modulate mRNA translation in plants (Liu et
503 al., 2012). Therefore, the effect of TOR kinase on *ATH1* is most likely indirect, as was recently
504 reported for WUS by Janocha et al. (2021) who show that TOR kinase indirectly induces *WUS*
505 expression by controlling cytokinin levels in the SAM through translational regulation of cytokinin
506 catabolic enzymes.
507 In the absence of light, *ATH1* gene expression is repressed by negative regulators of
508 photomorphogenesis, including COP1 (Quaedvlieg et al., 1995). This fits well with the observation
509 that in darkness COP1 represses TOR kinase (Chen et al., 2018). Here we report that, in darkness,
510 sucrose can substitute for light to induce *ATH1* expression and this also requires TOR kinase
511 activity (Figure 7). As sucrose-mediated induction of ATH1 can still be observed in a *cop1* mutant
512 background, sucrose affects TOR kinase activity most likely independently of COP1. Light
513 signaling inactivates COP1, resulting in an induction of auxin biosynthesis. Auxin then activates
514 the small Rho-like GTPase ROP2, which in turn activates TOR (Cai et al., 2017; Li et al., 2017;
515 Schepetilnikov et al., 2017). Constitutive expression of activated ROP2 stimulates TOR in the
516 shoot apex and is sufficient to promote organogenesis in the absence of light (Li et al., 2017).
517 Sugars are known to trigger the accumulation of auxin, along with its biosynthetic precursors and
518 this could be how sucrose activates TOR kinase in darkness, in the presence of COP1 (Chourey et
519 al., 2010; LeClere et al., 2010; Sairanen et al., 2012; Mohammed et al., 2017). Worth mentioning
520 in this respect is that the same set of PIF proteins that we identified as repressors of *ATH1*
521 expression, negatively regulate sugar-induced auxin biosynthesis (Sairanen et al., 2012).
522 In the presence of light, expression of *ATH1* is induced in a functionally redundant manner by
523 multiple cryptochrome and phytochrome photoreceptors operating in response to broad
524 wavelengths from blue to far-red light (Figure 7). This ensures presence of *ATH1* in the SAM

under all light conditions and thus inhibition of rib zone activity, resulting in the characteristic compact rosette growth habit of Arabidopsis plants. In line with this, loss of rosette habit has been observed in light-grown Arabidopsis plants lacking multiple functional phytochrome and/or cryptochrome photoreceptors. Control of vegetative internode elongation in response to changes in light quality or ambient temperature was shown to be mediated by the concerted action of phyA, phyB, phyD, phyE, and/or CRY1, all of which we identified here as having a role in light-mediated induction of *ATH1* expression (Devlin et al., 1996; Whitelam and Devlin, 1997; Devlin et al., 1998; Whitelam et al., 1998; Devlin et al., 1999; Mazzella et al., 2000; Devlin et al., 2003; Franklin et al., 2003a; Kanyuka et al., 2003; Strasser et al., 2010; Zhang et al., 2017). Often not appreciated in literature, compact rosette growth is thus a genuine photomorphogenic trait in Arabidopsis. Remarkably, rosette growth habit is a non-plastic trait, unlike other photoreceptor-driven developmental responses in Arabidopsis, such as elongation of hypocotyl, petiole, and inflorescence stem. A compact rosette habit is not affected in wildtype plants even under light quality conditions or temperature regimes that cause rapid elongation of aerial plant organs. Plasticity of growth and development is often considered adaptive, enabling sessile plants to adjust rapidly to a changing environment (Schlichting, 1986; Schlichting and Levin, 1986). However, as mentioned, rosette growth habit provides several advantages compared to a caulescent growth habit. Loss of a compact rosette in response to environmental cues, therefore, might be detrimental to plant fitness and viability. A compact rosette habit is not constitutively expressed in all rosette species (our unpublished observations) and this trait, as a result of selection, may have become fixed in Arabidopsis through genetic assimilation (Ehrenreich and Pfennig, 2016). Important contributors to genetic assimilation are genetic variants that alter gene regulation. Plausible ways in which gene regulation might facilitate loss of phenotypic plasticity are i) decoupling of the regulation of genes that control a plastic trait from environmental cues or ii) the evolution of additional regulatory pathways that makes their expression insensitive to the environment (Ehrenreich and Pfennig, 2016). The latter explanation (ii) might be true in the case of Arabidopsis rosette growth habit, given that *ATH1* expression is induced in response to broad wavelengths and involves multiple photoreceptors. Moreover, it has been proposed that ATH1 controls internode elongation by antagonizing a large number of genes that promote internode growth, mostly independent of each other (Ejaz et al., 2021). This assumption fits with the observation that *pifq* reduced internode elongation in *ath1-3* only by about 70%. Such multitarget control by ATH1 of

556 genes that affect internode elongation would further contribute to the robustness of rosette growth
557 habit in *A. thaliana*. Therefore, it is of interest to investigate whether ATH1 has a similar role in
558 other rosette species and, if so, whether differences in plasticity of rosette compactness can be
559 linked to differences in light-signaling control of *ATH1* expression and/or decoupling genes that
560 affect internode elongation from ATH1 regulation.
561 In this study, we identified *PIF1*, *PIF3*, *PIF4*, and *PIF5* as transcriptional targets of ATH1. Of
562 these, *PIF4* and several steps of the PIF pathway, were previously identified as a binding target of
563 ATH1 (Ejaz et al., 2021). Therefore, ATH1 might affect the expression of these four *PIF* genes
564 through direct transcriptional repression. Our finding that PIF4, and at least one of the other PIF
565 proteins, PIF1, PIF3, or PIF5, in turn function as negative regulators of *ATH1* expression suggest
566 the presence of a double-negative feedback loop between ATH1 and PIF family members (Figure
567 7). Signaling systems like ATH1 and PIFs that contain double-negative feedback loops can, in
568 principle, convert graded inputs into switch-like, irreversible responses (Ferrell, 2002). Such a
569 genetic toggle switch is a bistable dynamical system, possessing two stable equilibria, each
570 associated to a fully expressed protein. ATH1 has a fundamental role in maintaining the
571 Arabidopsis rosette habit during vegetative growth. When grown in the presence of light, *ATH1* is
572 expressed throughout the shoot meristem, including the subapical region where it represses stem
573 growth. Plant switching to reproductive growth rapidly downregulate *ATH1* at the shoot meristem,
574 marking the onset of bolting and emergence of an elongated inflorescence (Proveniers et al., 2007;
575 Gómez-Mena and Sablowski, 2008; Ejaz et al., 2021). Such stem elongation is absent in plants
576 constitutively expressing *ATH1,* without affecting formation of flowers (Cole et al., 2006; Gómez-
577 Mena and Sablowski, 2008; Rutjens et al., 2009). The data presented in this study show that both
578 absence of ATH1 and induced ATH1 expression, leads to pronounced changes in *PIF* gene
579 expression at the SAM associated with significant elongation or complete suppression of rosette
580 internodes, respectively. PIF proteins have been associated with bolting time and/or stem internode
581 elongation (Brock et al., 2010; Todaka et al., 2012; Galvão et al., 2019; Arya et al., 2021;
582 Jenkitkonchai et al., 2021). Moreover, elongated rosette internodes can be observed *35S::PIF4*
583 plants (see Figure 1d in Kumar et al. (2012)). It is therefore proposed that an ATH1-PIF toggle
584 switch underlies the rapid and distinctive switch in Arabidopsis growth habit that marks floral
585 transition.
586

Methods

Plant material and growth conditions

Arabidopsis seeds were obtained from the Nottingham Arabidopsis stock center (http://arabidopsis.info/; stock number between brackets) or were kind gifts of colleagues. The following genotypes were used: Col-8 wild type (N60000), L*er* wild-type (NW20), *phyB-5* (Reed et al., 1993), *phyBDE* (Shalitin et al., 2002), *phyABDE* (Franklin et al., 2003b), *phyBcry1* (Mazzella et al., 2000) *cry1-1* (Ahmad and Cashmore, 1993), *hy1-1* (Muramoto et al., 1999), *hy1cry1*, *hy1cry2*, *hy1cry1cry2* (López-Juez et al., 2008), *pif3-1* (N530753; Kim et al., 2003), *pif4-1* (N667486; Huai et al., 2018), *pif4pif5* (N68096; Leivar et al., 2012), *pif7-1* (N68809), *pif3pif4* (N66046), *pif1pif3* (N66045), *pif1pif3pif4* (N66500), *pif1pif3pif5* (N66047), *pif3pif4pif5* (N66048), *pif1pif3pif4pif5* (*pifq*; N66049) (Leivar et al., 2008), *cop1-4* (McNellis et al., 1994), *Pro35S:HA-ATH1*, *ATH1pro:GUS*, *ath1-3* (Proveniers et al., 2007), *ath1-4* (Li et al., 2012) and *35Spro:ATH1-HBD* lines (Rutjens et al., 2009), *35S::ALCR alcA:RNAi-TOR* and *35S:ALCR alcA:GUS* (Deprost et al., 2007).

To introduce *ATH1pro:GUS* in Col-8, L*er*, *phyB*, *phyBcry1*, and *phyBDE* backgrounds, the original *ATH1pro:GUS* line was crossed into the respective genotypes and the resulting offspring was backcrossed at least four times to the parental acceptor lines. For ectopic expression of *ATH1* in photoreceptor mutants, L*er*, *phyB*, *phyBcry1*, *phyBDE*, and *hy1cry1cry2* plants were transformed with a *HA*-tagged version of *ATH1* (*Pro35S:HA-ATH1*) as described previously (Proveniers et al., 2007). Transgenic seeds were selected based on seed GFP expression. Per genotype over ten independent, homozygous single insert lines were used for further analysis. To obtain *ath1-3 pifq* plants, F2 offspring plants from a cross *ath1-3* x *pifq* were preselected based on a, for higher-order *pif* mutants, characteristic short-petiole phenotype. Selected plants were then genotyped for homozygous presence of all five mutant alleles using the primers listed in Supplemental Table S2. To obtain *cop1-4 ath1-4* plants, F2 offspring plants from a cross *cop1-4* x *ath1-4*, homozygous for the *cop1* mutation, were selected under dark conditions for a short-hypocotyl phenotype. Subsequently, selected seedlings were transferred to normal growth conditions and genotyped for the *ath1-4* mutation.

For plant growth, seeds were chlorine gas sterilized in a desiccator for 4 h using a mixture of 4 ml 37% HCl and 100 ml commercial bleach (Glorix; contains 4.5% active chlorine) and put on soil (Primasta) or on sterile 0.8% plant agar (Duchefa Biochemie) with full strength Murashige-Skoog

618 medium (MS salts including MES Buffer (pH 5.8) and vitamins, Duchefa Biochemie) in square
619 Petri dishes (120x120 mm). After 2-3 days of stratification (4°C, darkness), plants were grown in
620 climate-controlled growth cabinets (Snijders, Microclima 1000) in either a short day (SD; 8 hours
621 light/16 hours dark) or a long day (LD; 16 hours light/8 hours dark) photoperiod, under 120 µmol
622 m^{-2} s^{-1} photosynthetic active radiation (PAR) fluorescent white-light conditions (Sylvania,
623 Luxline Plus Cool White) and 70% relative humidity. For growth of plants under monochromatic
624 light conditions, plants were grown in a Snijders Microclima growth cabinet equipped with Philips
625 GreenPower LEDs (red light (124.35 µmol m−2 s−1), blue light (6.14 µmol m−2 s−1) or far-red
626 light (77.57 µmol m−2 s−1)).
627 For liquid culture, Arabidopsis seedlings were grown in 100 mL bottles on a rotary shaker (185
628 rpm, 22 °C). Per bottle, ten to twenty seeds were added to 20 mL half-strength MS medium (MS
629 salts including MES Buffer (pH 5.8) and vitamins, Duchefa Biochemie) and bottles were sealed
630 with Steristoppers® (Heinz Herenz, Hamburg). After stratification, seeds were exposed to
631 fluorescent light (1-1.5 hours, 120 µmol/m2/s) to stimulate germination, after which the bottles
632 were wrapped in aluminum foil to avoid any further light exposure. Unless stated otherwise, sterile
633 sucrose (50% w/v) or sorbitol (50% w/v) was added to a final concentration of 1% v/v either at the
634 beginning or at day three of the experiment.
635
636 **Phenotypic analyses**
637 *Rosette internode elongation*
638 For light-grown plants, total rosette internode length was measured using a digital caliper. For
639 dark-grown seedlings, plants were photographed after three weeks of growth in liquid medium and
640 ImageJ (Schneider et al., 2012) was used to measure total rosette internode length. To determine
641 the average rosette internode length total rosette internode length was divided by the total number
642 of rosette leaves. In light-grown plants, the first leaf to give rise to a secondary inflorescence was
643 defined as the first cauline leaf. Dark-grown plants were never grown long enough to reach the
644 reproductive phase.
645 *Meristem cell size*
646 Using confocal laser scanning microscopy, longitudinal optical sections were made through apices
647 of five-day-old seedlings. In median sections a central cell file extending from the epidermis into
648 the subapical region where the hypocotyl vascular strands converge was identified. Using ImageJ

649 software ((NIH; https:imagej.nih.gov/ij/), individual cell lengths were then measured per position
650 in apical-basal direction.
651
652 **Gene expression analysis (qPCR)**
653 All samples (whole seedlings or SAM-enriched tissue) were snap-frozen in liquid N2 and stored
654 at -80°C before RNA extraction. For each experiment 3 or 4 biological replicates and two technical
655 replicates were included. RNA was isolated using a RNeasy mini or micro kit (Qiagen,
656 http://www.qiagen.com/). Genomic DNA was removed using DNaseI (Thermo Scientific) and
657 cDNA was synthesized from 500 ng - 1 µg RNA using RevertAid H Minus Reverse Transcriptase
658 and Ribolock RNAse inhibitor (Thermo Scientific) using a mix of anchored odT(20) primers (Jena
659 Bioscience) and random hexamers (IDT). qPCR reactions were performed using qPCRBIO
660 SyGreen Blue mix (PCRBIO) on a ViiA7 Real Time PCR system and ViiA7 software was used to
661 analyze the data. Relative expression levels were calculated using the ΔΔCt method (Livak and
662 Schmittgen, 2001), normalized to the expression of the reference genes *GAPC2* (AT1G13440)
663 and/or *MUSE3* (AT5G15400). Differences between mutant and wild-type ΔΔCt values were
664 statistically analyzed with an independent sample t-test or ANOVA test ($p < 0.05$) in Rstudio
665 version 1.2.5033. For primer sequences used, see Supplemental Table S1.
666
667 **β-Glucuronidase Staining and Microscopy**
668 Seven-day-old seedlings were harvested and vacuum-infiltrated in β-glucuronidase (GUS) staining
669 buffer (50 mM sodium phosphate buffer (pH=7.2), supplemented with 0.1% Triton X-100, 100
670 mM, potassium ferrocyanide, 100 mM, potassium ferricyanide, 2 mM 5-bromo-4-chloro-3-indolyl
671 glucuronide). Samples were incubated at room temperature for 16 hours and subsequently cleared
672 in ethanol baths with increasing concentration (20%, 30%, 50%, and 70%). Images were taken
673 with a Nikon DXMI200 camera attached to a Zeiss Stemi SV11 stereo microscope. The GUS
674 staining area in the shoot apex was measured and quantified using Image J (NIH;
675 https://imagej.nih.gov/ij/).
676
677 **Confocal microscopy**
678 Five-day-old Col-8, *ath1-4*, and *35Spro:ATH1-HBD* seedlings were grown in either continuous
679 darkness supplied with one percent sucrose or in continuous light at 27°C. Seedlings were cleared

using the ClearSee method (Kurihara et al., 2015) and imaged at a resolution of 0.25 x 0.25 x 0.5 µm using a Confocal Laser Scanning microscope Carl Zeiss LSM880 Fast AiryScan with a Plan-Apochromat 63x/1,2 Imm Korr DIC objective (numerical aperture 1.40, oil immersion) and ZEN software (blue edition, Carl Zeiss). Staining of apices with Calcofluor White Stain (Sigma-Aldrich) was performed as described before (Ursache et al., 2018). Excitation was at 405 nm and emission filters were set between 425 nm and 475 nm. All replicate images were acquired using identical confocal microscopy parameters for each experiment. Confocal images were processed with Fiji (version 1.52, Fiji) and Adobe Illustrator.

Statistical analysis

Data plotting and statistical analysis were performed using RSTUDIO.1.0.143 (www.rstudio.com) with R v.3.6.2 (https://cran.r-project.org/). The significance of differences between experimental groups was determined by using the student's t-test as indicated in each experiment. The significance level of differences between two experimental groups was either marked as *, $p<0.05$; **, $p<0.01$; ***, $p<0.001$; ns, not significant or indicated by the corresponding P values. In order to compare the significance of differences between multiple experimental groups, the Fisher's least significant difference (LSD) test and one-way analysis of variance (ANOVA) were performed using the Bonferroni correction with an $\alpha = 0.05$ from the agricolae package (Mendiburu, 2020). Images containing micrographs and other images were compiled using Adobe Illustrator and ImageJ software (https://imagej.nih.gov/ij/) to create the figures.

Author contributions

Conceptualization: M.P.; Methodology: M.P., S.S.H., S.S.S., and E.S.; Investigation: S.S.H., E.S., N.P., G.B., and S.S.S.; Writing – Original Draft: M.P. and S.S.H.; Writing – Review & Editing, M.P., S.S.H., S.S.S., E.S. and S.S.; Funding Acquisition: M.P., S.S.H., S.S. ; Visualization: S.S.H.; Resources: M.P., E.S., and S.S.; Supervision: M.P. and S.S.

Acknowledgements

phyA cry1, *phyB cry1* and *phyA phyB cry1* seeds were a kind gift of Jorge Casal. *hy1, cry1, cry2, cry1 cry2, hy1 cry1, hy1 cry2, and hy1 cry1 cry2* seeds were a kind gift of Enrique Lopez-Juez and *cop1-4* seeds were kind gift of Jan Lohmann.

References

Ahmad, M., and Cashmore, A. R. (1993). HY4 gene of A. thaliana encodes a protein with characteristics of a blue-light photoreceptor. *Nature* 366:162–166.

Araki, T., and Komeda, Y. (1993). Flowering in darkness in Arabidopsis thaliana. *Plant J* 4:801–811.

Arsovski, A. A., Galstyan, A., Guseman, J. M., and Nemhauser, J. L. (2012). Photomorphogenesis. *Arabidopsis Book* 2012:e0147.

Arya, H., Singh, M. B., and Bhalla, P. L. (2021). Overexpression of PIF4 affects plant morphology and accelerates reproductive phase transitions in soybean. *Food Energy Secur* 10.

Bello, F. D., Lepš, J., and Sebastià, M.-T. (2005). Predictive value of plant traits to grazing along a climatic gradient in the Mediterranean. *J Appl Ecol* 42:824–833.

Bencivenga, S., Serrano-Mislata, A., Bush, M., Fox, S., and Sablowski, R. (2016). Control of Oriented Tissue Growth through Repression of Organ Boundary Genes Promotes Stem Morphogenesis. *Dev Cell* 39:198–208.

Brock, M. T., Maloof, J. N., and Weinig, C. (2010). Genes underlying quantitative variation in ecologically important traits: PIF4 (PHYTOCHROME INTERACTING FACTOR 4) is associated with variation in internode length, flowering time, and fruit set in Arabidopsis thaliana. *Mol Ecol* 19:1187–1199.

Cai, W., Li, X., Liu, Y., Wang, Y., Zhou, Y., Xu, T., and Xiong, Y. (2017). COP1 integrates light signals to ROP2 for cell cycle activation. *Plant Signal Behav* 12:e1363946.

Chen, M., and Chory, J. (2011). Phytochrome signaling mechanisms and the control of plant development. *Trends Cell Biol* 21:664–671.

Chen, G.-H., Liu, M.-J., Xiong, Y., Sheen, J., and Wu, S.-H. (2018). TOR and RPS6 transmit light signals to enhance protein translation in deetiolating Arabidopsis seedlings. *Proc National Acad Sci* 115:12823–12828.

Chourey, P. S., Li, Q.-B., and Kumar, D. (2010). Sugar–Hormone Cross-Talk in Seed Development: Two Redundant Pathways of IAA Biosynthesis Are Regulated Differentially in the Invertase-Deficient miniature1 (mn1) Seed Mutant in Maize. *Mol Plant* 3:1026–1036.

Cole, M., Nolte, C., and Werr, W. (2006). Nuclear import of the transcription factor SHOOT MERISTEMLESS depends on heterodimerization with BLH proteins expressed in discrete sub-domains of the shoot apical meristem of Arabidopsis thaliana. *Nucleic Acids Res* 34:1281–1292.

745 Deng, X., and Quail, P. H. (1992). Genetic and phenotypic characterization of cop1 mutants of
746 Arabidopsis thaliana. *Plant J* 2:83–95.

747 Deprost, D., Yao, L., Sormani, R., Moreau, M., Leterreux, G., Nicolaï, M., Bedu, M., Robaglia,
748 C., and Meyer, C. (2007). The Arabidopsis TOR kinase links plant growth, yield, stress
749 resistance and mRNA translation. *Embo Rep* 8:864–870.

750 Devlin, P. F., Halliday, K. J., Harberd, N. P., and Whitelam, G. C. (1996). The rosette habit of
751 Arabidopsis thaliana is dependent upon phytochrome action: novel phytochromes control
752 internode elongation and flowering time. *Plant J* 10:1127–1134.

753 Devlin, P. F., Patel, S. R., and Whitelam, G. C. (1998). Phytochrome E Influences Internode
754 Elongation and Flowering Time in Arabidopsis. *Plant Cell* 10:1479–1487.

755 Devlin, P. F., Robson, P. R. H., Patel, S. R., Goosey, L., Sharrock, R. A., and Whitelam, G. C.
756 (1999). Phytochrome D Acts in the Shade-Avoidance Syndrome in Arabidopsis by Controlling
757 Elongation Growth and Flowering Time. *Plant Physiol* 119:909–916.

758 Devlin, P. F., Yanovsky, M. J., and Kay, S. A. (2003). A Genomic Analysis of the Shade
759 Avoidance Response in Arabidopsis . *Plant Physiol* 133:1617–1629.

760 Dong, P., Xiong, F., Que, Y., Wang, K., Yu, L., Li, Z., and Ren, M. (2015). Expression profiling
761 and functional analysis reveals that TOR is a key player in regulating photosynthesis and
762 phytohormone signaling pathways in Arabidopsis. *Front Plant Sci* 6:677.

763 Ehrenreich, I. M., and Pfennig, D. W. (2016). Genetic assimilation: a review of its potential
764 proximate causes and evolutionary consequences. *Ann Bot-london* 117:769–779.

765 Ejaz, M., Bencivenga, S., Tavares, R., Bush, M., and Sablowski, R. (2021). ARABIDOPSIS
766 THALIANA HOMEOBOX GENE 1 controls plant architecture by locally restricting
767 environmental responses. *Proc National Acad Sci* 118:e2018615118.

768 Ferrell, J. E. (2002). Self-perpetuating states in signal transduction: positive feedback, double-
769 negative feedback and bistability. *Curr Opin Cell Biol* 14:140–148.

770 Franklin, K. A., Praekelt, U., Stoddart, W. M., Billingham, O. E., Halliday, K. J., and Whitelam,
771 G. C. (2003a). Phytochromes B, D, and E Act Redundantly to Control Multiple Physiological
772 Responses in Arabidopsis. *Plant Physiol* 131:1340–1346.

773 Franklin, K. A., Davis, S. J., Stoddart, W. M., Vierstra, R. D., and Whitelam, G. C. (2003b). Mutant
774 Analyses Define Multiple Roles for Phytochrome C in Arabidopsis Photomorphogenesis. *Plant*
775 *Cell* 15:1981–1989.

776 Fujita, N., and Koda, R. (2015). Capitulum and rosette leaf avoidance from grazing by large
777 herbivores in Taraxacum. *Ecol Res* 30:517–525.

778 Galvão, V. C., Fiorucci, A.-S., Trevisan, M., Franco-Zorilla, J. M., Goyal, A., Schmid-Siegert, E.,
779 Solano, R., and Fankhauser, C. (2019). PIF transcription factors link a neighbor threat cue to
780 accelerated reproduction in Arabidopsis. *Nat Commun* 10:4005.

781 Gómez-Mena, C., and Sablowski, R. (2008). ARABIDOPSIS THALIANA HOMEOBOX GENE1
782 Establishes the Basal Boundaries of Shoot Organs and Controls Stem Growth. *Plant Cell*
783 20:2059–2072.

784 Huai, J., Zhang, X., Li, J., Ma, T., Zha, P., Jing, Y., and Lin, R. (2018). SEUSS and PIF4
785 Coordinately Regulate Light and Temperature Signaling Pathways to Control Plant Growth.
786 *Mol Plant* 11:928–942.

787 Jacqmard, A., Gadisseur, I., and Bernier, G. (2003). Cell Division and Morphological Changes in
788 the Shoot Apex of Arabidopsis thaliana during Floral Transition. *Ann. Bot.* 91:571–576.

789 Janocha, D., Pfeiffer, A., Dong, Y., Novák, O., Strnad, M., Ryabova, L. A., and Lohmann, J. U.
790 (2021). TOR kinase controls shoot development by translational regulation of cytokinin
791 catabolic enzymes. *Biorxiv* Advance Access published 2021, doi:10.1101/2021.07.29.454319.

792 Jenkitkonchai, J., Marriott, P., Yang, W., Sriden, N., Jung, J., Wigge, P. A., and Charoensawan,
793 V. (2021). Exploring PIF4's contribution to early flowering in plants under daily variable
794 temperature and its tissue-specific flowering gene network. *Plant Direct* 5:e339.

795 Kanyuka, K., Praekelt, U., Franklin, K. A., Billingham, O. E., Hooley, R., Whitelam, G. C., and
796 Halliday, K. J. (2003). Mutations in the huge Arabidopsis gene BIG affect a range of hormone
797 and light responses. *Plant J* 35:57–70.

798 Kathare, P. K., Xu, X., Nguyen, A., and Huq, E. (2020). A COP1-PIF-HEC regulatory module
799 fine-tunes photomorphogenesis in Arabidopsis. *Plant J* 104:113–123.

800 Kim, J., Yi, H., Choi, G., Shin, B., Song, P.-S., and Choi, G. (2003). Functional Characterization
801 of Phytochrome Interacting Factor 3 in Phytochrome-Mediated Light Signal Transduction.
802 *Plant Cell* 15:2399–2407.

803 Kumar, S. V., Lucyshyn, D., Jaeger, K. E., Alós, E., Alvey, E., Harberd, N. P., and Wigge, P. A.
804 (2012). Transcription factor PIF4 controls the thermosensory activation of flowering. *Nature*
805 484:242–245.

806 Kurihara, D., Mizuta, Y., Sato, Y., and Higashiyama, T. (2015). ClearSee: a rapid optical clearing
807 reagent for whole-plant fluorescence imaging. *Development* 142:4168–4179.

808 Larcher, W., Kainmüller, C., and Wagner, J. (2010). Survival types of high mountain plants under
809 extreme temperatures. *Flora - Morphol Distribution Funct Ecol Plants* 205:3–18.

810 LeClere, S., Schmelz, E. A., and Chourey, P. S. (2010). Sugar Levels Regulate Tryptophan-
811 Dependent Auxin Biosynthesis in Developing Maize Kernels . *Plant Physiol* 153:306–318.

812 Leivar, P., Monte, E., Oka, Y., Liu, T., Carle, C., Castillon, A., Huq, E., and Quail, P. H. (2008).
813 Multiple Phytochrome-Interacting bHLH Transcription Factors Repress Premature Seedling
814 Photomorphogenesis in Darkness. *Curr Biol* 18:1815–1823.

815 Leivar, P., Tepperman, J. M., Cohn, M. M., Monte, E., Al-Sady, B., Erickson, E., and Quail, P. H.
816 (2012). Dynamic Antagonism between Phytochromes and PIF Family Basic Helix-Loop-Helix
817 Factors Induces Selective Reciprocal Responses to Light and Shade in a Rapidly Responsive
818 Transcriptional Network in Arabidopsis. *Plant Cell* 24:1398–1419.

819 Li, L., and Sheen, J. (2016). Dynamic and diverse sugar signaling. *Curr Opin Plant Biol* 33:116–
820 125.

821 Li, Y., Pi, L., Huang, H., and Xu, L. (2012). ATH1 and KNAT2 proteins act together in regulation
822 of plant inflorescence architecture. *J Exp Bot* 63:1423–1433.

823 Li, X., Cai, W., Liu, Y., Li, H., Fu, L., Liu, Z., Xu, L., Liu, H., Xu, T., and Xiong, Y. (2017).
824 Differential TOR activation and cell proliferation in Arabidopsis root and shoot apexes. *Proc*
825 *National Acad Sci* 114:2765–2770.

826 Liu, M., Wu, S., Chen, H., and Wu, S. (2012). Widespread translational control contributes to the
827 regulation of Arabidopsis photomorphogenesis. *Mol Syst Biol* 8:566–566.

828 Livak, K. J., and Schmittgen, T. D. (2001). Analysis of Relative Gene Expression Data Using
829 Real-Time Quantitative PCR and the 2−ΔΔC T Method. *Methods* 25:402–408.

830 López-Juez, E., Dillon, E., Magyar, Z., Khan, S., Hazeldine, S., Jager, S. M. de, Murray, J. A. H.,
831 Beemster, G. T. S., Bögre, L., and Shanahan, H. (2008). Distinct Light-Initiated Gene
832 Expression and Cell Cycle Programs in the Shoot Apex and Cotyledons of Arabidopsis . *Plant*
833 *Cell* 20:947–968.

834 Ma, D., Li, X., Guo, Y., Chu, J., Fang, S., Yan, C., Noel, J. P., and Liu, H. (2016). Cryptochrome
835 1 interacts with PIF4 to regulate high temperature-mediated hypocotyl elongation in response
836 to blue light. *Proc National Acad Sci* 113:224–229.

837 Mazzella, M. A., Bertero, D., and Casal, J. J. (2000). Temperature-dependent internode elongation
838 in vegetative plants of Arabidopsis thaliana lacking phytochrome B and cryptochrome 1. *Planta*
839 210:497–501.

840 McNellis, T. W., Arnim, A. G. von, Araki, T., Komeda, Y., Miséra, S., and Deng, X. W. (1994).
841 Genetic and molecular analysis of an allelic series of cop1 mutants suggests functional roles
842 for the multiple protein domains. *Plant Cell* 6:487–500.

843 Menand, B., Desnos, T., Nussaume, L., Berger, F., Bouchez, D., Meyer, C., and Robaglia, C.
844 (2002). Expression and disruption of the Arabidopsis TOR (target of rapamycin) gene. *Proc*
845 *National Acad Sci* 99:6422–6427.

Mendiburu, F. de (2020). Statistical Procedures for Agricultural Research Package "agricolae" (1.3-3). The R Project for Statistical Computing. https://cran.r-project.org/package=agricolae Advance Access published 2020.

Mohammed, B., Bilooei, S. F., Dóczi, R., Grove, E., Railo, S., Palme, K., Ditengou, F. A., Bögre, L., and López-Juez, E. (2017). Converging Light, Energy and Hormonal Signaling Control Meristem Activity, Leaf Initiation, and Growth . *Plant Physiol* 176:1365–1381.

Montané, M.-H., and Menand, B. (2013). ATP-competitive mTOR kinase inhibitors delay plant growth by triggering early differentiation of meristematic cells but no developmental patterning change. *J Exp Bot* 64:4361–4374.

Muramoto, T., Kohchi, T., Yokota, A., Hwang, I., and Goodman, H. M. (1999). The Arabidopsis Photomorphogenic Mutant hy1 Is Deficient in Phytochrome Chromophore Biosynthesis as a Result of a Mutation in a Plastid Heme Oxygenase. *Plant Cell* 11:335–347.

Patil, I. (2021). Visualizations with statistical details: The "ggstatsplot" approach. *J Open Source Softw* 6:3167.

Pedmale, U. V., Huang, S. C., Zander, M., Cole, B. J., Hetzel, J., Ljung, K., Reis, P. A. B., Sridevi, P., Nito, K., Nery, J. R., et al. (2016). Cryptochromes Interact Directly with PIFs to Control Plant Growth in Limiting Blue Light. *Cell* 164:233–245.

Peterson, R. L., and Yeung, E. C. (1972). Effect of Two Gibberellins on Species of the Rosette Plant Hieracium. *Bot Gaz* 133:190–198.

Pfeiffer, A., Janocha, D., Dong, Y., Medzihradszky, A., Schöne, S., Daum, G., Suzaki, T., Forner, J., Langenecker, T., Rempel, E., et al. (2016). Integration of light and metabolic signals for stem cell activation at the shoot apical meristem. *Elife* 5:e17023.

Pham, V. N., Kathare, P. K., and Huq, E. (2018a). Dynamic regulation of PIF5 by COP1–SPA complex to optimize photomorphogenesis in Arabidopsis. *Plant J* 96:260–273.

Pham, V. N., Kathare, P. K., and Huq, E. (2018b). Phytochromes and Phytochrome Interacting Factors. *Plant Physiol* 176:1025–1038.

Pham, V. N., Xu, X., and Huq, E. (2018c). Molecular bases for the constitutive photomorphogenic phenotypes in Arabidopsis. *Development* 145:dev169870.

Ponnu, J., and Hoecker, U. (2021). Illuminating the COP1/SPA Ubiquitin Ligase: Fresh Insights Into Its Structure and Functions During Plant Photomorphogenesis. *Front Plant Sci* 12:662793.

Proveniers, M., Rutjens, B., Brand, M., and Smeekens, S. (2007). The Arabidopsis TALE homeobox gene ATH1 controls floral competency through positive regulation of FLC. *Plant J* 52:899–913.

879 Quaedvlieg, N., Dockx, J., Rook, F., Weisbeek, P., and Smeekens, S. (1995). The homeobox gene
880 ATH1 of Arabidopsis is derepressed in the photomorphogenic mutants cop1 and det1. *Plant*
881 *Cell* 7:117–129.

882 Rabot, A., Henry, C., Baaziz, K. B., Mortreau, E., Azri, W., Lothier, J., Hamama, L., Boummaza,
883 R., Leduc, N., Pelleschi-Travier, S., et al. (2012). Insight into the Role of Sugars in Bud Burst
884 Under Light in the Rose. *Plant Cell Physiol* 53:1068–1082.

885 Reed, J. W., Nagpal, P., Poole, D. S., Furuya, M., and Chory, J. (1993). Mutations in the gene for
886 the red/far-red light receptor phytochrome B alter cell elongation and physiological responses
887 throughout Arabidopsis development. *Plant Cell* 5:147–157.

888 Roldán, M., Gómez-Mena, C., Ruiz-García, L., Salinas, J., and Martínez-Zapater, J. M. (1999).
889 Sucrose availability on the aerial part of the plant promotes morphogenesis and flowering of
890 Arabidopsis in the dark. *Plant J* 20:581–590.

891 Rutjens, B., Bao, D., Eck-Stouten, E. V., Brand, M., Smeekens, S., and Proveniers, M. (2009).
892 Shoot apical meristem function in Arabidopsis requires the combined activities of three BEL1-
893 like homeodomain proteins. *Plant J* 58:641–654.

894 Sachs, R. M., Bretz, C. F., and Lang, A. (1959). SHOOT HISTOGENESIS: THE EARLY
895 EFFECTS OF GIBBERELLIN UPON STEM ELONGATION IN TWO ROSETTE PLANTS.
896 *Am J Bot* 46:376–384.

897 Sairanen, I., Novák, O., Pěnčík, A., Ikeda, Y., Jones, B., Sandberg, G., and Ljung, K. (2012).
898 Soluble Carbohydrates Regulate Auxin Biosynthesis via PIF Proteins in Arabidopsis . *Plant*
899 *Cell* 24:4907–4916.

900 Schaffer, W. M., and Schaffer, M. V. (1979). The Adaptive Significance of Variations in
901 Reproductive Habit in the Agavaceae II: Pollinator Foraging Behavior and Selection for
902 Increased Reproductive Expenditure. *Ecology* 60:1051–1069.

903 Schepetilnikov, M., and Ryabova, L. A. (2017). Recent Discoveries on the Role of TOR (Target
904 of Rapamycin) Signaling in Translation in Plants. *Plant Physiol* 176:1095–1105.

905 Schepetilnikov, M., Makarian, J., Srour, O., Geldreich, A., Yang, Z., Chicher, J., Hammann, P.,
906 and Ryabova, L. A. (2017). GTPase ROP2 binds and promotes activation of target of
907 rapamycin, TOR, in response to auxin. *Embo J* 36:886–903.

908 Schlichting, Carl. D. (1986). The evolution of phenotypic plasticity in plants. *Ann. Rev. of Ecol.*
909 *Syst* 17:667–693.

910 Schlichting, C. D., and Levin, D. A. (1986). Phenotypic plasticity: an evolving plant character.
911 *Biol J Linn Soc* 29:37–47.

912 Schneider, C. A., Rasband, W. S., and Eliceiri, K. W. (2012). NIH Image to ImageJ: 25 years of
913 image analysis. *Nat Methods* 9:671–675.

914 Serrano-Mislata, A., Bencivenga, S., Bush, M., Schiessl, K., Boden, S., and Sablowski, R. (2017).
915 DELLA genes restrict inflorescence meristem function independently of plant height. *Nat*
916 *Plants* 3:749–754.

917 Shalitin, D., Yang, H., Mockler, T. C., Maymon, M., Guo, H., Whitelam, G. C., and Lin, C. (2002).
918 Regulation of Arabidopsis cryptochrome 2 by blue-light-dependent phosphorylation. *Nature*
919 417:763–767.

920 Strasser, B., Sánchez-Lamas, M., Yanovsky, M. J., Casal, J. J., and Cerdán, P. D. (2010).
921 Arabidopsis thaliana life without phytochromes. *Proc National Acad Sci* 107:4776–4781.

922 Thomson, F. J., Moles, A. T., Auld, T. D., and Kingsford, R. T. (2011). Seed dispersal distance is
923 more strongly correlated with plant height than with seed mass. *J Ecol* 99:1299–1307.

924 Todaka, D., Nakashima, K., Maruyama, K., Kidokoro, S., Osakabe, Y., Ito, Y., Matsukura, S.,
925 Fujita, Y., Yoshiwara, K., Ohme-Takagi, M., et al. (2012). Rice phytochrome-interacting
926 factor-like protein OsPIL1 functions as a key regulator of internode elongation and induces a
927 morphological response to drought stress. *Proc National Acad Sci* 109:15947–15952.

928 Ursache, R., Andersen, T. G., Marhavý, P., and Geldner, N. (2018). A protocol for combining
929 fluorescent proteins with histological stains for diverse cell wall components. *Plant J* 93:399–
930 412.

931 Vaughan, J. G. (1955). The morphology and growth of the vegetative and reproductive apices of
932 Arabidopsis thaliana (L.) Heynh., Capsella bursa-pastoris (L.) Medic. and Anagallis arvensis
933 L. *J Linn Soc Lond Botany* 55:279–301.

934 Whitelam, G. C., and Devlin, P. F. (1997). Roles of different phytochromes in Arabidopsis
935 photomorphogenesis. *Plant Cell Environ* 20:752–758.

936 Whitelam, G. C., Patel, S., and Devlin, P. F. (1998). Phytochromes and photomorphogenesis in
937 Arabidopsis. *Philosophical Transactions Royal Soc Lond Ser B Biological Sci* 353:1445–1453.

938 Wu, Q., Kuang, K., Lyu, M., Zhao, Y., Li, Y., Li, J., Pan, Y., Shi, H., and Zhong, S. (2020).
939 Allosteric deactivation of PIFs and EIN3 by microproteins in light control of plant
940 development. *Proc National Acad Sci* 117:18858–18868.

941 Xiong, Y., McCormack, M., Li, L., Hall, Q., Xiang, C., and Sheen, J. (2013). Glucose–TOR
942 signalling reprograms the transcriptome and activates meristems. *Nature* 496:181–186.

943 Xu, X., Paik, I., Zhu, L., Bu, Q., Huang, X., Deng, X. W., and Huq, E. (2014). PHYTOCHROME
944 INTERACTING FACTOR1 Enhances the E3 Ligase Activity of CONSTITUTIVE

PHOTOMORPHOGENIC1 to Synergistically Repress Photomorphogenesis in Arabidopsis . *Plant Cell* 26:1992–2006.

Zhang, B., Holmlund, M., Lorrain, S., Norberg, M., Bakó, L., Fankhauser, C., and Nilsson, O. (2017). BLADE-ON-PETIOLE proteins act in an E3 ubiquitin ligase complex to regulate PHYTOCHROME INTERACTING FACTOR 4 abundance. *Elife* 6:e26759.

Figure legends

Figure 1: ***ATH1* expression is sufficient to restore compact rosette growth in dark-grown Arabidopsis plants**

A: Average rosette internode elongation in dark-grown Col-8, *ath1-3*, and *35Spro:ATH1-HBD* plants treated with 0.1% ethanol (mock) or 10 µM dexamethasone (Dex). Sucrose was added three days after the start of the experiment.

B: Representative three-week-old, dark-grown plants used in A. Arrows indicate elongated rosette internodes, the arrowhead indicates suppression of internode elongation. Scale bars denote 2 mm.

C: Relative expression of *ATH1* in Col-8 plants grown for either five, ten, or fifteen days (d) in continuous light or continuous darkness at 22°C. Sucrose was present at a one percent final concentration from the beginning of the experiment. Transcript levels were normalized to *MUSE3* (AT5G15400). The average of three biological replicates is shown. Error bars represent standard deviation of the ΔCT mean. P-values indicate significant differences; p-value < 0.05, p-value < 0.01, and p-value < 0.001 are represented by "*", "**", "***" respectively.

D: Relative expression of *ATH1* in seven-day-old seedlings grown in continuous light (+) or continuous darkness (-) in the presence (+) or absence (-) of one percent sucrose. Transcript levels were normalized to *GAPC2* (AT1G13440). The average of three biological replicates is shown. The p-value for the observed difference is depicted in the figure.

E: GUS-stained seven-day-old, dark-grown *ATH1pro:GUS* seedlings in the absence (0%) or presence (0.5% and 1%) of sucrose. GUS activity is visible as a blue precipitate. Scale bars represent 0.01 mm.

F: Average rosette internode elongation in three-week-old dark-grown Col-8 and *35Spro:ATH1-HBD* plants treated with increasing concentrations of Dex (0 nM to 10 µM).

G: Average rosette internode elongation of three-week-old dark-grown Col-8 and *ath1-4* seedlings treated with increasing concentrations of sucrose (0.5 to 2.5%).

In **A** and **G**: Different letters indicate statistically significant differences (P< 0.05) as determined by one-way analysis of variance with Tukey's honest significant difference post hoc test. In **A**: The p-value for the observed difference in *35Spro:ATH1-HBD* (mock and Dex) is depicted in the figure. In **A**, **F**, **G**: colored dots indicate rosette internode elongation scores of individual seedlings.

Figure 2: **Sugar-induced dark-grown seedlings display a SAM morphology similar to light-grown *ath1* mutants**

Median longitudinal optical sections through the shoot apical meristems of five-day-old Col-8 (**A, B**), *ath1-4* (**C**), and *35Spro:ATH1-HBD* (**D, E)** seedlings grown at 27°C in the presence (**A**, **C**) or absence (**B**, **D**, **E**) of light. Mock treatment (**D**) is 0.1% ethanol, Dex treatment (**E**) is 10 µM dexamethasone. Cells marked in red form a central cell file extending from the epidermis into the subapical region that forms the rib zone. Scale bars represent 10 µm. **F**: Quantification of cell lengths as illustrated in **A-E**. Individual cell lengths were measured per position in apical-basal direction. Per genotype and condition four or five individual apices were analyzed. The numbers on the x-axis correspond to the cell position as depicted in **A-E**.

Figure 3: Significant reduction in *ATH1* expression levels underlies loss of rosette habit in photoreceptor mutants

A: Expression of *ATH1* in seven-day-old seedlings (L*er*) grown in SD white light (WL), red (RL), blue (BL), far-red light (FRL) or continuous darkness (DRK). Transcript levels were normalized to *GAPC2* (AT1G13440). Dots indicate the average values of four biological replicates per light treatment, each consisting of 40-50 seedlings.

B: Shoot apices of GUS-stained, seven-day-old $ATH1_{pro}$:GUS seedlings in different genetic backgrounds (Col-8, *phyB*, *phyBcry1*, and *phyBDE*). Plants were grown in whit light under short-day conditions. Scale bars represent 0.01 mm.

C: Heat map generated from qPCR data on relative *ATH1* expression in indicated photoreceptor mutants (see **Figure S1**), when compared to wild-type control plants (L*er*). Transcript levels were normalized to *GAPC2* (AT1G13440; BL) or *MUSE3* (AT5G15400; RL, FRL and WL). The average of three biological replicates is shown. At least 20 shoot apices were used for each biological replicate. Red corresponds to high relative expression and dark blue corresponds to low relative expression. A linear fold change scale is displayed on top.

D: Average rosette internode elongation in WT (L*er*), *phyB*, *phyBcry1*, *hy1cry1*, and *hy1cry1cry2* in the absence or presence of a *Pro_{35S}:HA-ATH1* transgene. Plants were grown under LD conditions. Different letters denote statistically significant differences between groups ($P < 0.05$) as determined by 1-way ANOVA followed by Tukey's post hoc test. Colored dots indicate the average rosette internode length per individual ($n \geq 16$ individual plants per genotype).

E: Representative plants from **D**. Arrows indicate elongated rosette internodes, the arrowheads indicate complete suppression of internode elongation. Scale bars represent 5 mm.

Figure 4: Derepression of *ATH1* contributes to a compact rosette habit in dark-grown *cop1* mutants

A: Relative mRNA abundance of *ATH1* in shoot apices of two-week-old dark-grown seedlings. The average of three biological replicates is shown. At least 20 shoot apices were used for each biological replicate. The p-value of significant differences, as determined by the two-tailed Student's t-test, are indicated in the figure.

B: Average rosette internode lengths of 3-week-old Col-8, *ath1-4*, *cop1-4,* and *cop-1 ath1-4* plants (n ≥13) grown in continuous darkness for three weeks at 22°C, in the presence of one percent sucrose.

The significant differences are indicated in the figure as determined by Pairwise test Games-Howell according to R package ggstatsplot (Patil, 2021).

C: Representative plants from **B**. Arrows indicate elongated rosette internodes, arrowheads indicate complete suppression of internode elongation. Scale bars represent 0.5 mm.

Sucrose (Suc +) or sorbitol (Suc -), both to a final concentration of one percent, were added three days after start of the experiment (**A**, **C**)

Figure 5: **A double-negative feedback loop between ATH1 and PIFs is required for initiation and maintenance of rosette growth habit**

A: Average internode lengths of 3-week-old Col-8, *pif3*, *pif4*, *pif7*, *pif1pif3*, *pif3pif4*, *pif4pif5*, *pif1pif3pif4*, *pif1pif3pif5*, *pif3pif4pif5*, and *pifq* (*pif1pif3pif4pif5*) plants grown in continuous darkness at 22°C. Sucrose was added to the medium to a final concentration of one percent three days after the start of the experiment. Colored dots indicate average rosette internode elongation scores of individual seedlings (n ≥9). *The p-value* of significant differences compared to wild type Col-8, as determined by the two-tailed Student's t-test, are indicated in the figure.

B: Relative mRNA abundance of *ATH1* in SAM-enriched tissue of 14-day-old, dark-grown Col-8, *pif4*, and *pifq* seedlings (n≥20 per biological replicate; four biological replicates). Transcript levels were normalized to *GAPC2* (AT1G13440). The p-value of significant differences, as

determined by the two-tailed Student's t-test, are indicated in the figure. Sucrose was present at a one percent final concentration from the start of the experiment.

C: Average internode lengths of three-week-old Col-8, *pif4*, *pifq*, and *pifq ath1-3* plants grown in continuous darkness at 22°C. Sucrose was added to the medium to a final concentration of one percent three days after the start of the experiment. The p-value of significant differences, as determined by the two-tailed Student's t-test, are indicated in the figure. Colored dots indicate average rosette internode elongation scores of individual seedlings (n ≥11).

D, **E**: Relative mRNA abundance of indicated *PIF* genes in SAM-enriched tissue of 14-day-old, dark-grown Col-8 and *35Spro:ATH1-HBD* (n ≥3) (**D**) or 39-day-old, light-grown (SD conditions) Col-8 and *ath1-3* seedlings (n ≥2) (**E**). For (**D**) seedlings were treated with a mock (0.1% ethanol, Dex -) or 10 µM dexamethasone (Dex +) at day three, and in total, 30-40 shoot apices were used for each biological replicate (**D**). For light-grown plants (**E**), three shoot apices were used per biological replicate. Transcript levels were normalized to *GAPC2* (AT1G13440). Seedlings were treated with a mock (0.1% ethanol, Dex -) or 10 µM dexamethasone (Dex +) (**D**). The p-value of significant differences, as determined by the two-tailed Student's t-test, are indicated in the figures.

Figure 6: ***ATH1* expression is independently regulated by light and sucrose**

A: Schematic representation of the experimental setup. *ATH1$_{pro}$:GUS* seeds were light-treated for 45 minutes to stimulate germination, before growth in continuous darkness for five days. AZD-8055, lincomycin, norflurazon, or NaOH + CaO were then added and seedings were grown for an additional five hours in darkness before switching to *ATH1*-inducing conditions (continuous light or continued growth in darkness in the presence of sucrose (Suc)) for two more days.

B: Shoot apices of GUS-stained *ATH1$_{pro}$:GUS* seedlings treated with either NaOH + CaO, 0.5 mM lincomycin, or 5 µM norflurazon according to the scheme depicted in (**A**). Mock-treatment was with ethanol to a final concentration of 0.1%. Scale bars represent 0.05 mm.

C: Relative expression of *ATH1* in seven-day-old, dark-grown seedlings, grown in the presence of either sucrose, glucose, fructose, palatinose, or sorbitol, all at a final concentration of one percent in the growth medium. Sugars were added at the start of the experiment. Transcript levels were normalized to *MUSE3* (At5g15400). The average of three biological replicates is shown. At least 30 seedlings were used for each biological replicate.

D, E: Shoot apices of GUS-stained *ATH1$_{pro}$:GUS* seedlings treated with the TOR kinase inhibitor AZD-8055 before switching to ATH1-inducing conditions (continuous light (**D**) or darkness in the presence of one percent sucrose (**E**)) according to the scheme depicted in (**A**). Scale bars represent 0.01 mm.

F: Relative expression of *ATH1* in seven-day-old, dark-grown *35S::ALCR alcA:RNAi-TOR* and *35S:ALCR alcA:GUS* (control line) seedlings in the presence or absence of ethanol (ETOH; 0.1%) and/or sucrose (Suc; 1%). Experimental setup was as in (**A**). ETOH was added after five days of growth in darkness. After an additional five hours in darkness sucrose was added and plants were sampled after two more days in darkness. Transcript levels were normalized to *GAPC2* (AT1G13440). The average of three biological replicates is shown. At least 30 seedlings were used for each biological replicate. Different letters denote statistically significant differences between groups ($P < 0.05$) as determined by 1-way ANOVA followed by Tukey's post hoc test.

Figure 7: Light and sucrose signaling pathways converge at TOR kinase to control *ATH1* expression and subsequent rosette growth habit in *Arabidopsis thaliana*.

Expression of *ATH1* is mediated by the activity of TOR kinase in response to both sugar and light. In response to light (**left panel**), photoreceptor signaling inhibits the activity of a COP1-containing protein complex that acts as a central repressor of light signaling in darkness. This releases the inhibitory effect of COP1 on TOR kinase. Activation of TOR kinase then leads to both activation of the SAM and induction of *ATH1* expression in the SAM. As a consequence of *ATH1* expression in the SAM, *PIF* gene expression, including *PIF4*, is locally inhibited. This contributes to inhibition of rib zone activity and, consequently, suppression of rosette internode elongation with the for Arabidopsis typical rosette growth habit as a result. As TOR kinase is a major regulator of mRNA translation, the effect on *ATH1* expression is most likely indirect (dotted arrow). In the absence of light (**right panel**), the COP1-complex is stabilized and inhibits TOR kinase activity and subsequent SAM activation. In addition, the COP1-complex stabilizes PIFs in darkness to positively regulate skotomorphogenesis. As a combined effect, *ATH1* is not expressed under these conditions. Sucrose-availability to the SAM can substitute for light both in the case of SAM activation and for *ATH1* induction. Although both processes are mediated through TOR kinase, sucrose levels sufficient to activate the SAM only result in weak expression of *ATH1*, probably as the result of still active COP1-PIF signaling. Resulting ATH1 levels are insufficient to suppress

rib zone activity. As a consequence, in most circumstances sugar-induced dark-grown seedlings display a caulescent growth habit due to premature rib zone activation resulting in elongation of vegetative internodes.

Figure S1: **Relative mRNA abundance of ATH1 in different photoreceptor mutants**

A-D: Relative expression of *ATH1* in seven-day-old wild type (L*er*) and indicated photoreceptor mutants grown under SD conditions in the presence of white light (**A**), red light (**B**), blue light (**C**) or far-red light (**D**). Transcript levels were normalized to *GAPC2* (AT1G13440) (BL) or *MUSE3* (AT5G15400; WL, RL, and FRL). Data shown are the average of three biological replicates. At least 30 seedlings were used for each biological replicate. Different letters denote statistically significant differences between groups ($P < 0.05$) as determined by 1-way ANOVA followed by Tukey's post hoc test.

Figure S2: **Sugar-induced dark-grown seedlings phenocopy light-grown *ath1*mutants**

Rosette elongation phenotypes of wild-type Col-8 (**A** and **B**) *ath1-4* (**C**), and *35Spro:ATH1-HBD* (*ATH1-HBD*; **D** and **E**) plants grown in the presence (**A**, **C**) or absence (**B**, **D**, **E**) of light at 27°C. *35Spro:ATH1-HBD* plants were treated either with a mock (0.1% ethanol, **D**) or 10 µM dexamethasone (Dex, **E**). Dark-grown plants (**B**, **D**, **E**) were supplemented with sucrose to a final concentration of one percent three days after the start of the experiment. Arrows indicate elongated rosette internodes, the arrowhead indicates complete suppression of internode elongation.

F: Average rosette internode lengths of plants depicted in **A**-**E**. Per genotype and treatment 10 individual plants were analyzed. Scale bars represent 5 mm.

Figure S3: ***ATH1$_{pro}$:GUS* activity in seven-day-old seedlings grown in darkness in the presence of different sugars**

A, B: Quantification of GUS-staining intensity in *ATH1$_{pro}$:GUS* shoot apices from **Figure 5B, E**. Different letters denote statistically significant differences between groups ($P < 0.05$) as determined by 1-way ANOVA followed by Tukey's post hoc test.

C: Shoot apices of GUS-stained *ATH1$_{pro}$:GUS* seedlings grown in continuous darkness for seven days. Plants were grown in the presence of either sucrose, glucose, fructose, palatinose, or sorbitol,

all added to the growth medium to a final concentration of one percent at the start of the experiment. Scale bars represent 0.05 mm.

Figure S4: **Effect of TOR inhibition on *ATH1* expression in *cop1-4* mutant seedlings.**

Relative expression of *ATH1* in seven-day-old *cop1-4* mutants grown according to the experimental setup indicated in **Figure 5A**. Seeds were light-treated for 45 minutes to stimulate germination and then grown in continuous darkness for five days. Following the addition of AZD-8055, the seedlings were grown for two more days in darkness before samples were taken. Transcript levels were normalized to *MUSE3* (AT5G15400). The average of three (AZD-8055 -) or four (AZD-8055 +) biological replicates is shown. At least 30 seedlings were used for each biological replicate. The p-value of significant difference, as determined by the two-tailed Student's t-test, is indicated in the figure.

Figures

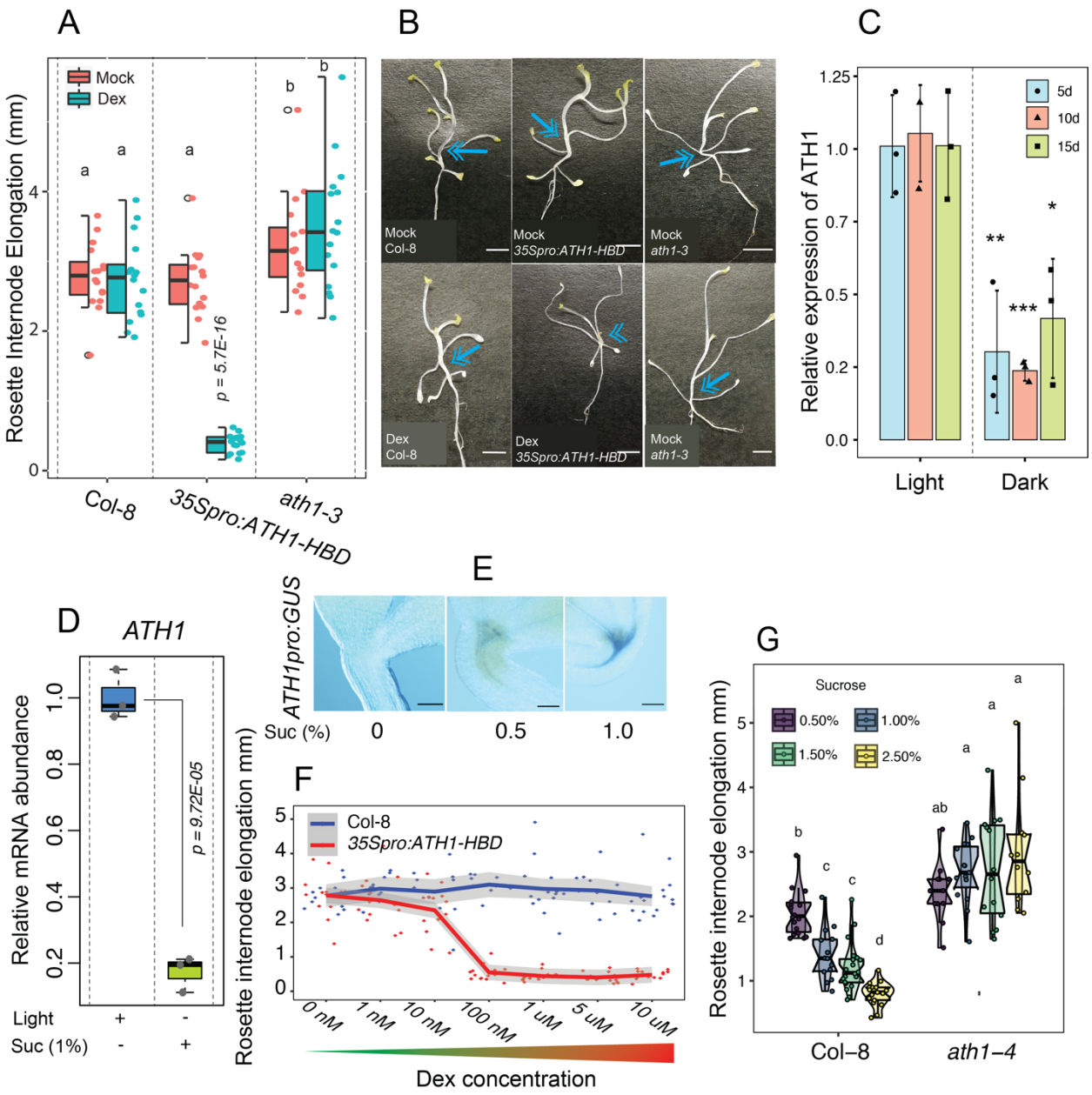

Figure 1: ***ATH1*** **expression is sufficient to restore compact rosette growth in dark-grown Arabidopsis plants**

A: Average rosette internode elongation in dark-grown Col-8, *ath1-3*, and *35Spro:ATH1-HBD* plants treated with 0.1% ethanol (mock) or 10 µM dexamethasone (Dex). Sucrose was added three days after the start of the experiment. **B:** Representative three-week-old, dark-grown plants used in A. Arrows indicate elongated rosette internodes, the arrowhead indicates suppression of internode elongation. Scale bars denote 2 mm. **C**: Relative expression of *ATH1* in Col-8 plants grown for either 5, 10, or 15 days (d) in continuous light or continuous darkness at 22°C. Sucrose was present at a one percent final concentration from the beginning of the experiment. Transcript

levels were normalized to *MUSE3* (AT5G15400). The average of three biological replicates is shown. Error bars represent standard deviation of the ΔCT mean. p-values indicate significant differences; p-value < 0.05, p-value < 0.01, and p-value < 0.001 are represented by "*", "**", "***" respectively. **D**: Relative expression of *ATH1* in seven-day-old seedlings grown in continuous light (+) or continuous darkness (-) in the presence (+) or absence (-) of one percent sucrose. Transcript levels were normalized to *GAPC2* (AT1G13440). The average of three biological replicates is shown. The p-value for the observed difference is depicted in the figure. **E:** GUS-stained 7-day-old, dark-grown *ATH1pro:GUS* seedlings in the absence (0%) or presence (0.5% and 1%) of sucrose. GUS activity is visible as a blue precipitate. Scale bars represent 0.01 mm. **F**: Average rosette internode elongation in three-week-old dark-grown Col-8 and *35Spro:ATH1-HBD* plants treated with increasing concentrations of Dex (0 nM to 10 μM). **G**: Average rosette internode elongation of three-week-old dark-grown Col-8 and *ath1-4* seedlings treated with increasing concentrations of sucrose (0.5 to 2.5%). In **A** and **G**: Different letters indicate statistically significant differences ($p < 0.05$) as determined by one-way analysis of variance with Tukey's honest significant difference post hoc test. In **A**: The p-value for the observed difference in *35Spro:ATH1-HBD* (mock and Dex) is depicted in the figure. In **A**, **F**, **G**: colored dots indicate rosette internode elongation scores of individual seedlings.

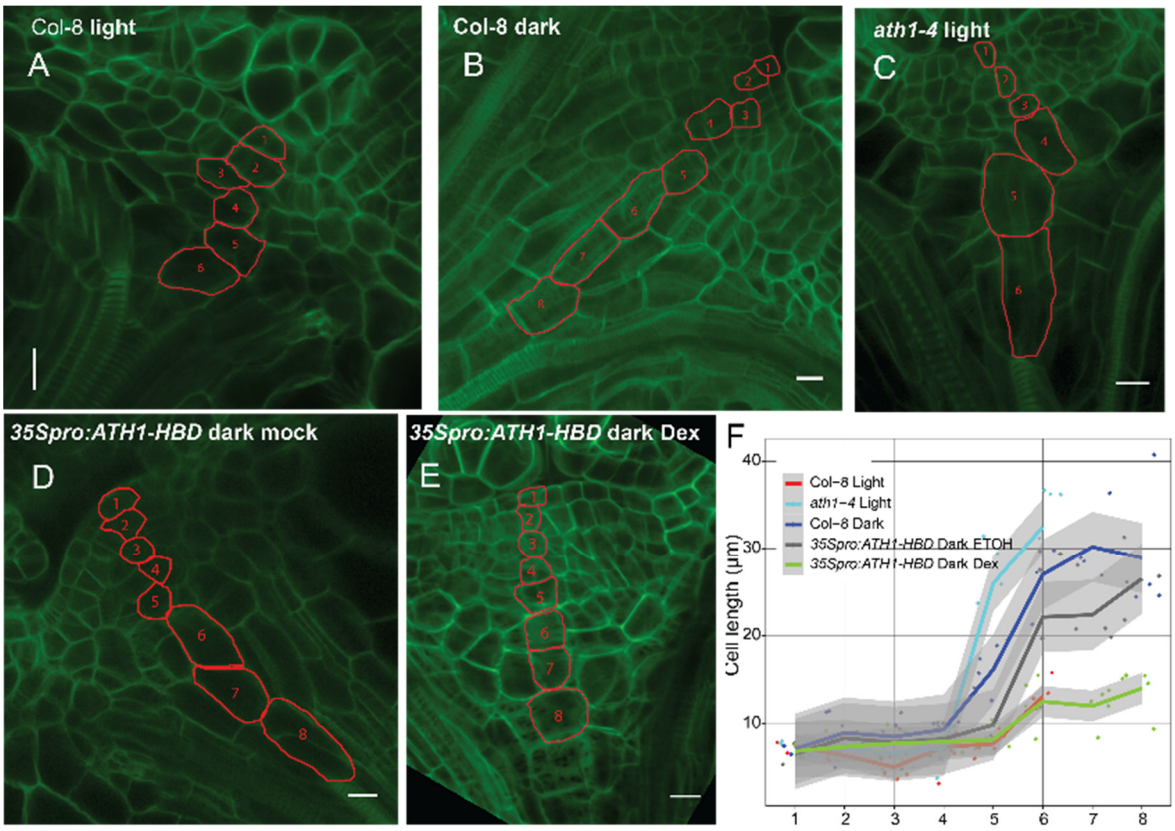

Figure 2: **Sugar-induced dark-grown seedlings display a SAM morphology similar to light-grown *ath1* mutants**

Median longitudinal optical sections through the shoot apical meristems of five-day-old Col-8 (**A, B**), *ath1-4* (**C**), and *35Spro:ATH1-HBD* (**D, E**) seedlings grown at 27°C in the presence (**A**, **C**) or absence (**B**, **D**, **E**) of light. Mock treatment (**D**) is 0.1% ethanol, Dex treatment (**E**) is 10 µM dexamethasone. Cells marked in red form a central cell file extending from the epidermis into the subapical region that forms the rib zone. Scale bars represent 10 µm. **F**: Quantification of cell lengths as illustrated in **A-E**. Individual cell lengths were measured per position in apical-basal direction. Per genotype and condition four or five individual apices were analyzed. The numbers on the x-axis correspond to the cell position as depicted in **A-E**.

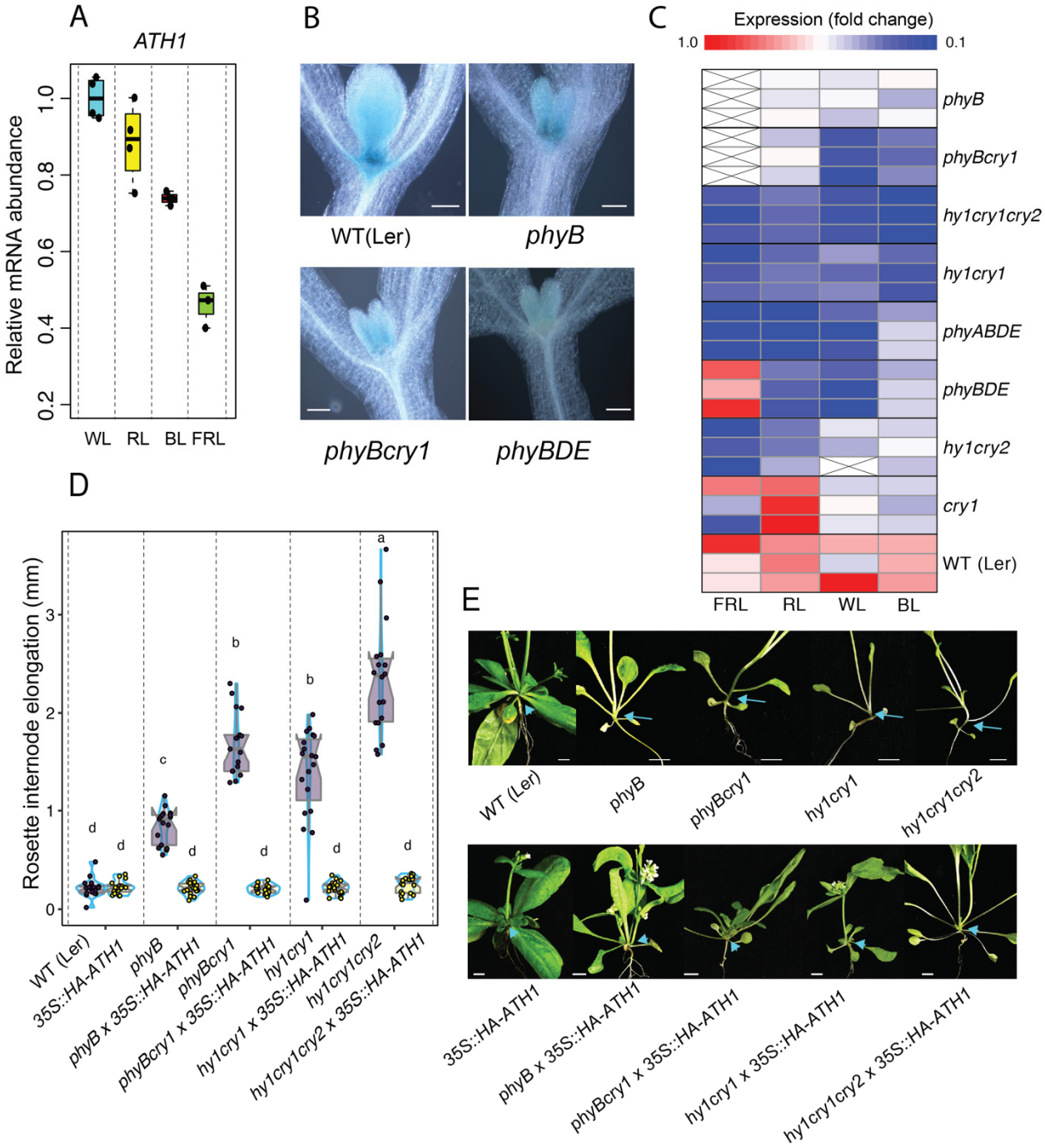

Figure 3: Significant reduction in *ATH1* expression levels underlies loss of rosette habit in photoreceptor mutants

A: Expression of *ATH1* in seven-day-old seedlings (L*er*) grown in SD white light (WL), red (RL), blue (BL), far-red light (FRL), or continuous darkness (DRK). Transcript levels were normalized to *GAPC2* (AT1G13440). Dots indicate the average values of four biological replicates per light treatment, each consisting of 40-50 seedlings. **B**: Shoot apices of GUS-stained, seven-day-old *ATH1*$_{pro}$:GUS seedlings in different genetic backgrounds (Col-8, *phyB*, *phyBcry1*, and *phyBDE*). Plants were grown in whit light under short-day conditions. Scale bars represent 0.01 mm. **C**: Heat

map generated from qPCR data on relative *ATH1* expression in indicated photoreceptor mutants (see **Figure S1**), when compared to wild-type control plants (L*er*). Transcript levels were normalized to *GAPC2* (AT1G13440; BL) or *MUSE3* (AT5G15400; RL, FRL and WL). The average of three biological replicates is shown. At least 20 shoot apices were used for each biological replicate. Red corresponds to high relative expression and dark blue corresponds to low relative expression. A linear fold change scale is displayed on top. **D:** Average rosette internode elongation in WT (L*er*), *phyB*, *phyBcry1*, *hy1cry1*, and *hy1cry1cry2* in the absence or presence of a *Pro$_{35S}$:HA-ATH1* transgene. Plants were grown under LD conditions. Different letters denote statistically significant differences between groups ($p < 0.05$) as determined by 1-way ANOVA followed by Tukey's post hoc test. Colored dots indicate the average rosette internode length per individual ($n \geq 16$ individual plants per genotype). **E:** Representative plants from **D**. Arrows indicate elongated rosette internodes, the arrowheads indicate complete suppression of internode elongation. Scale bars represent 5 mm.

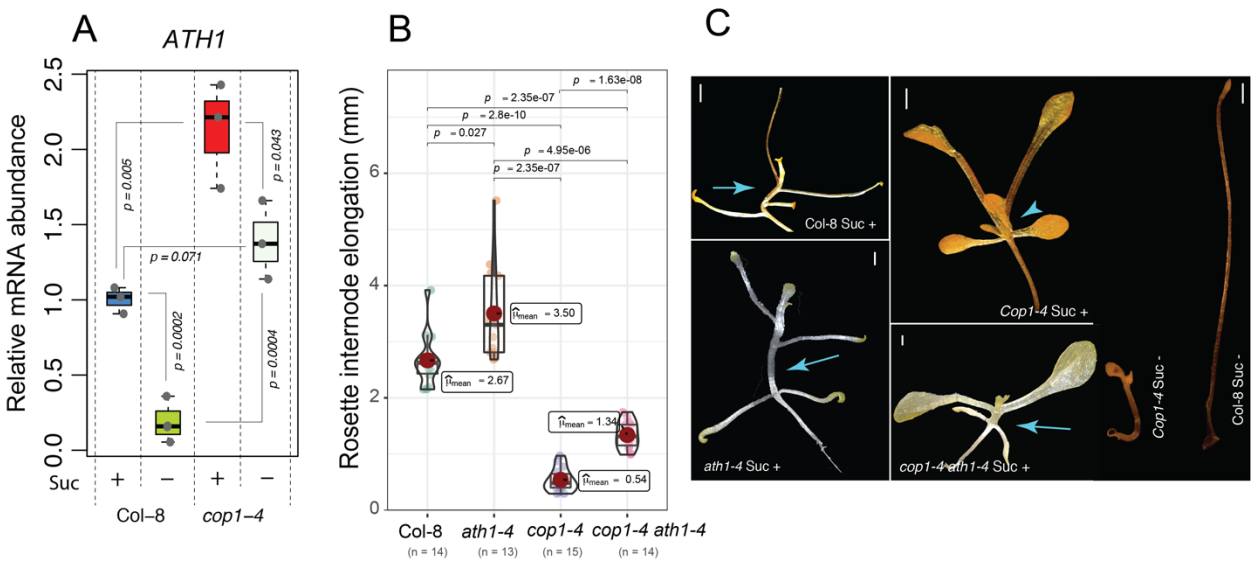

Figure 4: Derepression of *ATH1* contributes to a compact rosette habit in dark-grown *cop1* mutants

A: Relative mRNA abundance of *ATH1* in shoot apices of two-week-old dark-grown seedlings. The average of three biological replicates is shown. At least 20 shoot apices were used for each biological replicate. The p-value of significant differences, as determined by the two-tailed Student's t-test, are indicated in the figure. **B:** Average rosette internode lengths of three-week-old Col-8, *ath1-4*, *cop1-4,* and *cop-1 ath1-4* plants (n ≥13) grown in continuous darkness for three weeks at 22°C, in the presence of one percent sucrose. The significant differences are indicated in the figure as determined by Pairwise test Games-Howell according to R package ggstatsplot (Patil, 2021). **C**: Representative plants from **B**. Arrows indicate elongated rosette internodes, the arrowhead indicates complete suppression of internode elongation. Scale bars represent 0.5 mm. Sucrose (Suc +) or sorbitol (Suc -), both to a final concentration of one percent, were added three days after start of the experiment (**A**, **C**)

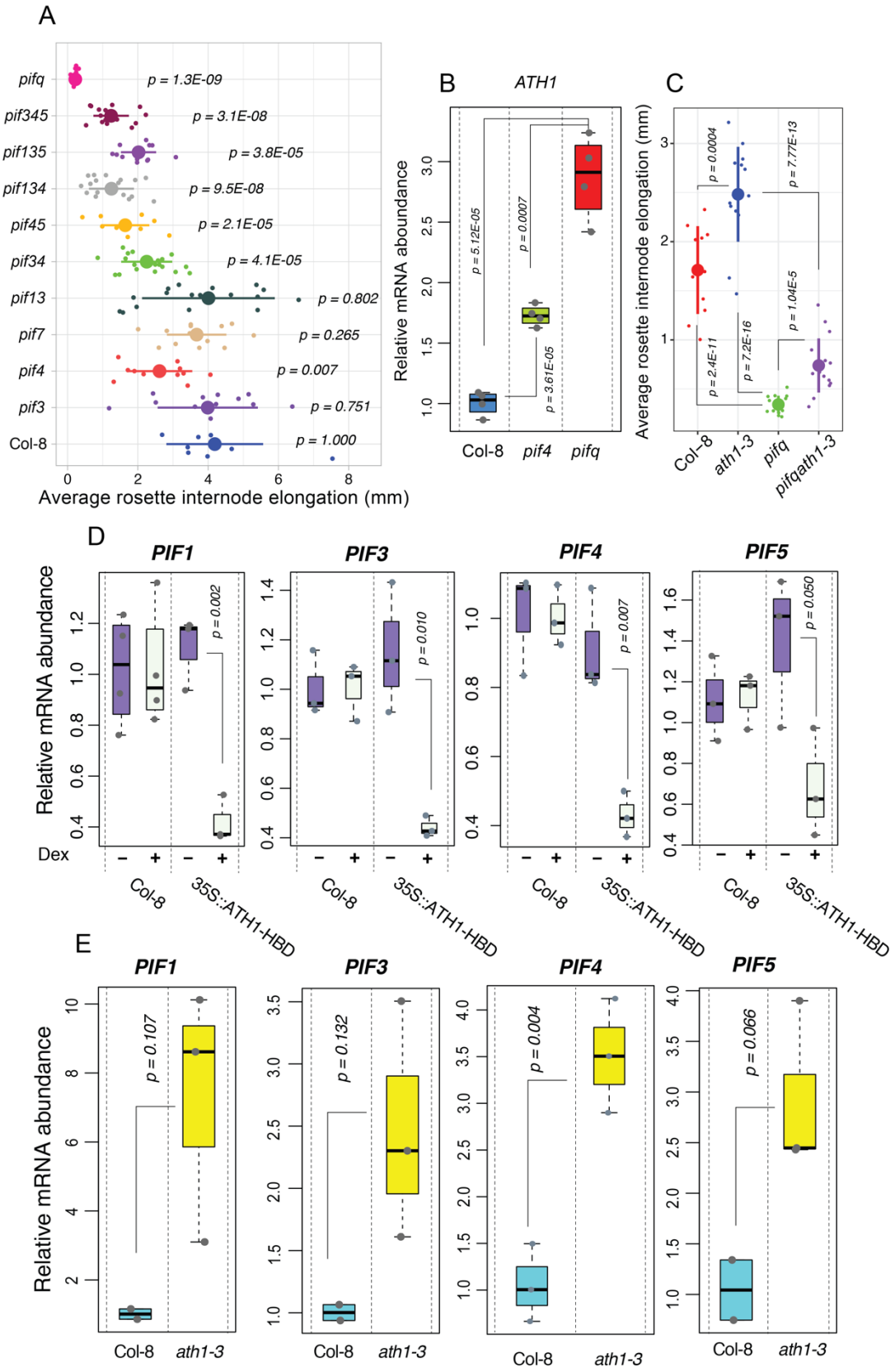

Figure 5: **A double-negative feedback loop between ATH1 and PIFs is required for initiation and maintenance of rosette growth habit**

A: Average internode lengths of 3-week-old Col-8, *pif3*, *pif4*, *pif7*, *pif1pif3*, *pif3pif4*, *pif4pif5*, *pif1pif3pif4*, *pif1pif3pif5*, *pif3pif4pif5*, and *pifq* (*pif1pif3pif4pif5*) plants grown in continuous darkness at 22°C. Sucrose was added to the medium to a final concentration of one percent three days after the start of the experiment. Colored dots indicate average rosette internode elongation scores of individual seedlings (n ≥9). The p-value of significant differences compared to wild type Col-8, as determined by the two-tailed Student's t-test, are indicated in the figure. **B**: Relative mRNA abundance of *ATH1* in SAM-enriched tissue of 14-day-old, dark-grown Col-8, *pif4*, and *pifq* seedlings (n≥20 per biological replicate; four biological replicates). Transcript levels were normalized to *GAPC2* (AT1G13440). The p-value of significant differences, as determined by the two-tailed Student's t-test, are indicated in the figure. Sucrose was present at a one percent final concentration from the start of the experiment. **C**: Average internode lengths of three-week-old Col-8, *pif4*, *pifq*, and *pifq ath1-3* plants grown in continuous darkness at 22°C. Sucrose was added to the medium to a final concentration of one percent three days after the start of the experiment. The p-value of significant differences, as determined by the two-tailed Student's t-test, are indicated in the figure. Colored dots indicate average rosette internode elongation scores of individual seedlings (n ≥11). **D**, **E**: Relative mRNA abundance of indicated *PIF* genes in SAM-enriched tissue of 14-day-old, dark-grown Col-8 and *35Spro:ATH1-HBD* (n ≥3) (**D**) or 39-day-old, light-grown (SD conditions) Col-8 and *ath1-3* seedlings (n ≥2) (**E**). For (**D**) seedlings were treated with a mock (0.1% ethanol, Dex -) or 10 μM dexamethasone (Dex +) at day three, and in total, 30-40 shoot apices were used for each biological replicate (**D**). For light-grown plants (**E**), three shoot apices were used per biological replicate. Transcript levels were normalized to *GAPC2* (AT1G13440). Seedlings were treated with a mock (0.1% ethanol, Dex -) or 10 μM dexamethasone (Dex +) (**D**). The p-value of significant differences, as determined by the two-tailed Student's t-test, are indicated in the figures.

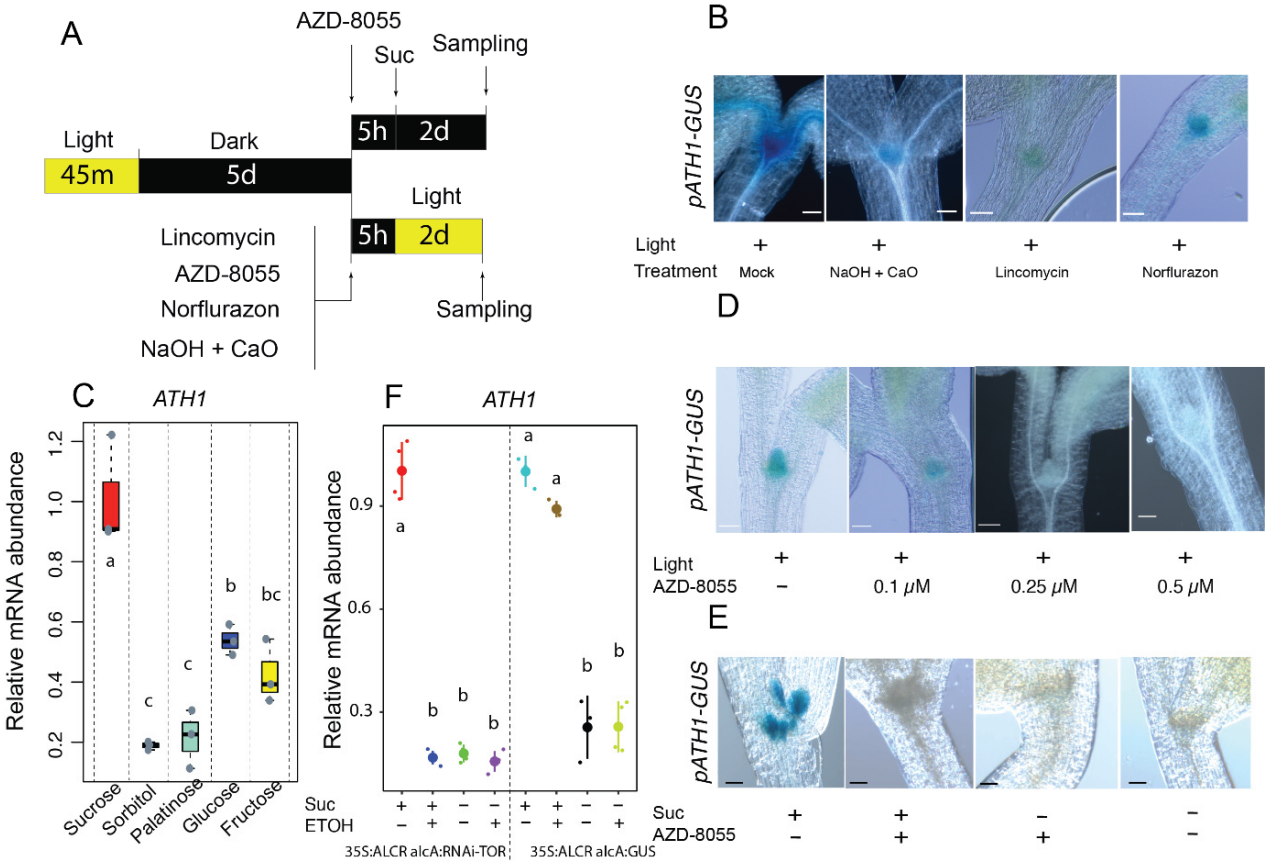

Figure 6: ***ATH1* expression is independently regulated by light and sucrose**

A: Schematic representation of the experimental setup. *ATH1*$_{pro}$*:GUS* seeds were light-treated for 45 minutes to stimulate germination, before growth in continuous darkness for five days. AZD-8055, lincomycin, norflurazon, or NaOH + CaO were then added and seedings were grown for an additional five hours in darkness before switching to *ATH1*-inducing conditions (continuous light or continued growth in darkness in the presence of sucrose (Suc)) for two more days. **B**: Shoot apices of GUS-stained *ATH1*$_{pro}$*:GUS* seedlings treated with either NaOH + CaO, 0.5 mM lincomycin, or 5 μM norflurazon according to the scheme depicted in (**A**). Mock-treatment was with ethanol to a final concentration of 0.1%. Scale bars represent 0.05 mm. **C**: Relative expression of *ATH1* in seven-day-old, dark-grown seedlings, grown in the presence of either sucrose, glucose, fructose, palatinose, or sorbitol, all at a final concentration of one percent in the growth medium. Sugars were added at the start of the experiment. Transcript levels were normalized to *MUSE3* (At5g15400). The average of three biological replicates is shown. At least 30 seedlings were used for each biological replicate. **D, E**: Shoot apices of GUS-stained *ATH1*$_{pro}$*:GUS* seedlings treated with the TOR kinase inhibitor AZD-8055 before switching to ATH1-inducing conditions (continuous light (**D**) or darkness in the presence of one percent sucrose (**E**)) according to the scheme depicted in (**A**). Scale bars represent 0.01 mm. **F**: Relative expression of *ATH1* in seven-day-old, dark-grown *35S::ALCR alcA:RNAi-TOR* and *35S:ALCR alcA:GUS* (control line) seedlings in the presence or absence of ethanol (ETOH; 0.1%) and/or sucrose (Suc; 1%). Experimental setup was as in (**A**). ETOH was added after five days of growth in darkness. After an additional 5 hours in darkness sucrose was added and plants were sampled after two more days in darkness. Transcript levels were normalized to *GAPC2* (AT1G13440). The average of three

biological replicates is shown. At least 30 seedlings were used for each biological replicate. Different letters denote statistically significant differences between groups ($p < 0.05$) as determined by 1-way ANOVA followed by Tukey's post hoc test.

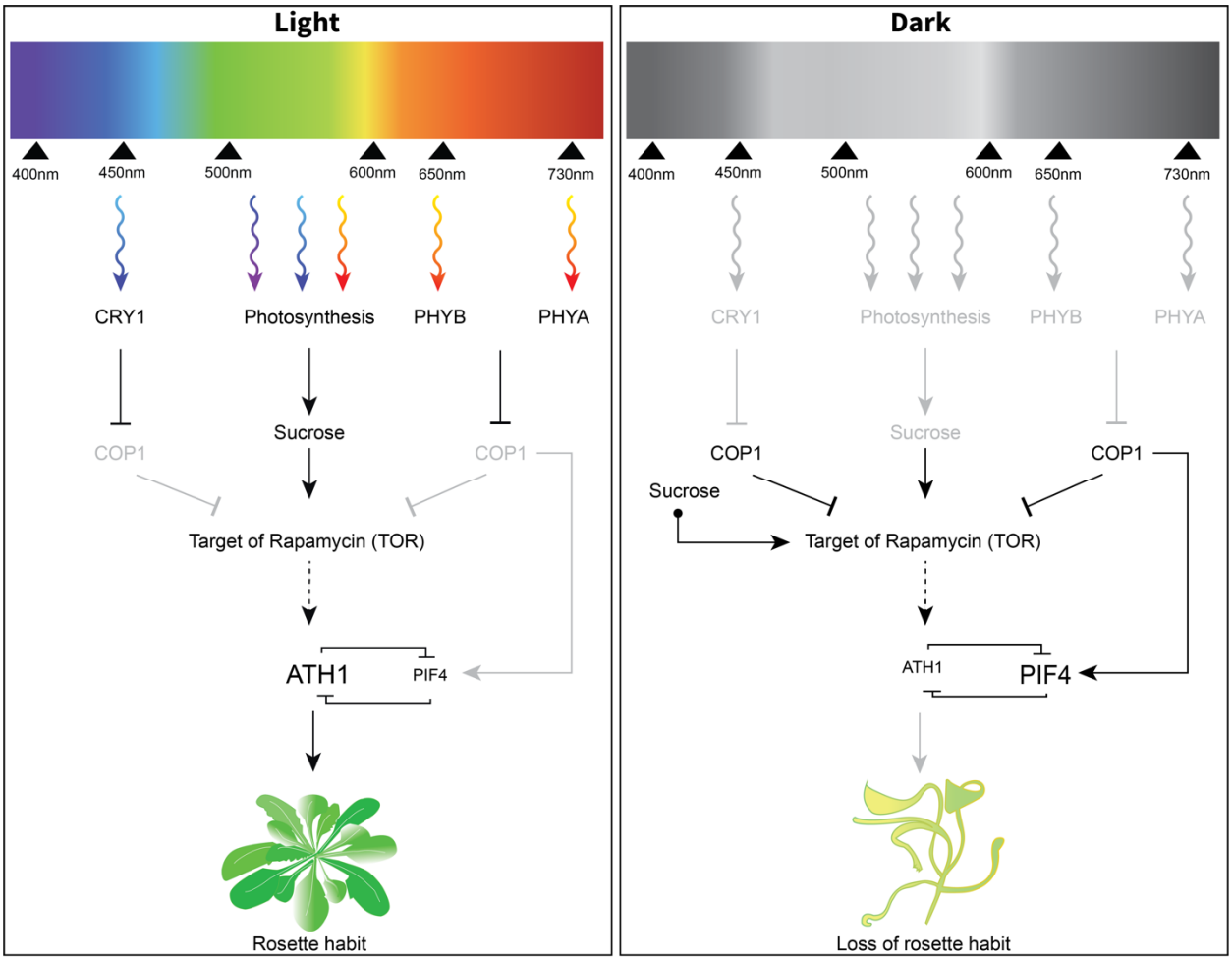

Figure 7: Light and sucrose signaling pathways converge at TOR kinase to control *ATH1* expression and subsequent rosette growth habit in *Arabidopsis thaliana*.
Expression of *ATH1* is mediated by the activity of TOR kinase in response to both sugar and light. In response to light (**left panel**), photoreceptor signaling inhibits the activity of a COP1-containing protein complex that acts as a central repressor of light signaling in darkness. This releases the inhibitory effect of COP1 on TOR kinase. Activation of TOR kinase then leads to both activation of the SAM and induction of *ATH1* expression in the SAM. As a consequence of *ATH1* expression in the SAM, *PIF* gene expression, including *PIF4*, is locally inhibited. This contributes to inhibition of rib zone activity and, consequently, suppression of rosette internode elongation with the for Arabidopsis typical rosette growth habit as a result. As TOR kinase is a major regulator of mRNA translation, the effect on *ATH1* expression is most likely indirect (dotted arrow). In the absence of light (**right panel**), the COP1-complex is stabilized and inhibits TOR kinase activity and subsequent SAM activation. In addition, the COP1-complex stabilizes PIFs in darkness to positively regulate skotomorphogenesis. As a combined effect, *ATH1* is not expressed under these conditions. Sucrose-availability to the SAM can substitute for light both in the case of SAM activation and for *ATH1* induction. Although both processes are mediated through TOR kinase, sucrose levels sufficient to activate the SAM only result in weak expression of *ATH1*, probably as the result of still active COP1-PIF signaling. Resulting ATH1 levels are insufficient to suppress rib zone activity. As a consequence, in most circumstances sugar-induced dark-grown seedlings

display a caulescent growth habit due to premature rib zone activation resulting in elongation of vegetative internodes.

Supplemental Information

Supplemental Table S1: Primers for qRT-PCR**.**

Gene	Sequence Fw	Sequence Rv	Ref,.
ATH1 (AT4G32980)	CAACGAGGTTTGCCTGAGAAA	TTCGGGTAAGGGTGAAGGAA	
PIF1 (AT2G20180)	TGAATCCCGTAGCGAGGAAACAA	TTCCACATCCCATTGACATCATCTG	(Xu et al., 2017)
PIF3 (AT1G09530)	CTGAAAGGAGACGGCGTGATAG	CAGATAGTAACCAGACGCCATTGAC	(Zhong et al., 2012)
PIF4 (AT2G43010)	CAGCTTCAAGTGATGTGGATG	CATAACCGGAAATCGAGGTAA	(Qi et al., 2020)
PIF5 (AT3G59060)	CAACTCCAAGTGATGTGGATG	CAATTGCATCTGACTTTGCAT	(Qi et al., 2020)
MUSE3 (AT5G15400)	GGGCACTCAAGTATCTTGTTAGC	TGCTGCCCAACATCAGGTT	(Pei et al., 2007)
GAPC2 (AT1G13440)	TTGGTGACAACAGGTCAAGCA	AAACTTGTCGCTCAATGCAATC	(Czechowski et al., 2005)

Supplemental Table S2: Primers for genotyping.

Gene	Left primer (LP)	Right primer (RP)	Ref., & notes
pif1-1 (SAIL_256_G07)	LP: AAGGAAGGAGGAGGAATAGGC	RP: CATGAATTTCTCGAGGCTGAG	(Sparks et al., 2016)
	LB: GCTTCCTATTATATCTTCCCAAATTACCAATACA		
pif3-7	A: GGTCACCATGCTCCAACTCT	B: CCTGAGAAAGTAGGCGGAGA	1
	C: TCTCCGCCTACTTTCTCAGG	D: TGTTGCGTTTTACAGAAACAATC	
pif3-1 (SALK_030753)	LP: AGTCTGTTGCTTCTGCTACGC	RP: TTGCATAAGGCATTCCCATAC	
	LB: ATTTTGCCGATTTCGGAAC		
pif4-2 (SAIL_1288_E07)	LP: ACCTCCTCAAGTCATGGTTAAGCCTAAGCC	RP: TCCAAACGAGAACCGTCGGT	(Leivar et al., 2008b)
	LB: TAGCATCTGAATTTCATAACCAATCTCGATACAC		
pif5-3 (SALK_087012)	LP: CGATTTGTTACCCATGGTTTG	RP: CCTTGCTCGATTTTTGTTACG	(Sparks et al., 2016)
	LB: ATTTTGCCGATTTCGGAAC		
pif7-1	LP: CCGTTCATGGTCTAGGCG	RP: CATCCTCTGGTTTATCCTATCACGCCG	(Leivar et al., 2008b)
	LB: TGATAGTGACCTTAGGCGACTTTTGAACGC		
ah1-3 (SALK_113353)	LP: CGCTCGATTATTCATCTCGAG	RP: CACTCTATATCATTTGCCCGC	
	LB: ATTTTGCCGATTTCGGAAC		
ath1-4	ATH1int-F: CCGAGTTAGATCCACAGTTACA	ATH1int-R: CATTTCCGCATACATCTCTTC	2

1: WT (A + B = 248bp, A + D = 784bp, C + D = 132bp); *pif3-7* (A + B = no band, A + D = no band, C + D = 132bp)

2: *ath1-4* is an EMS mutant (TGG-> TGA, CDS nt1170). The ATH1int-F and ATH1int-R primers generate PCR amplicons of 905 bp containing the *ath1-4* SNP. In wild-type plants, BseGI results in two fragments (259 and 648 bp) of the amplicon while the *ath1-4* mutant remains uncut.

Supplemental figures

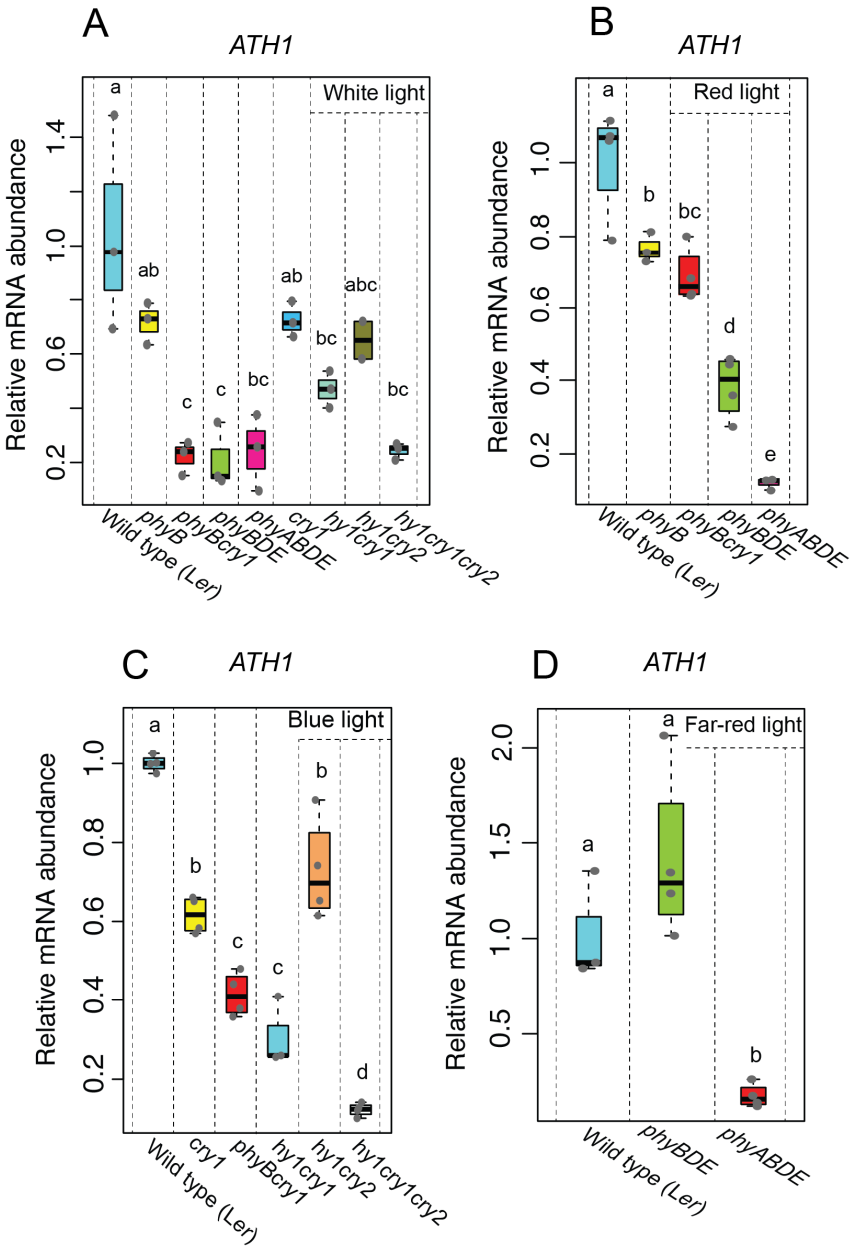

Figure S1: **Relative mRNA abundance of ATH1 in different photoreceptor mutants**
A-D: Relative expression of *ATH1* in seven-day-old wild type (L*er*) and indicated photoreceptor mutants grown under SD conditions in the presence of white light (**A**), red light (**B**), blue light (**C**) or far-red light (**D**). Transcript levels were normalized to *GAPC2* (AT1G13440) (BL) or *MUSE3* (AT5G15400; WL, RL, and FRL). Data shown are the average of three biological replicates. At least 30 seedlings were used for each biological replicate. Different letters denote statistically significant differences between groups ($p < 0.05$) as determined by 1-way ANOVA followed by Tukey's post hoc test.

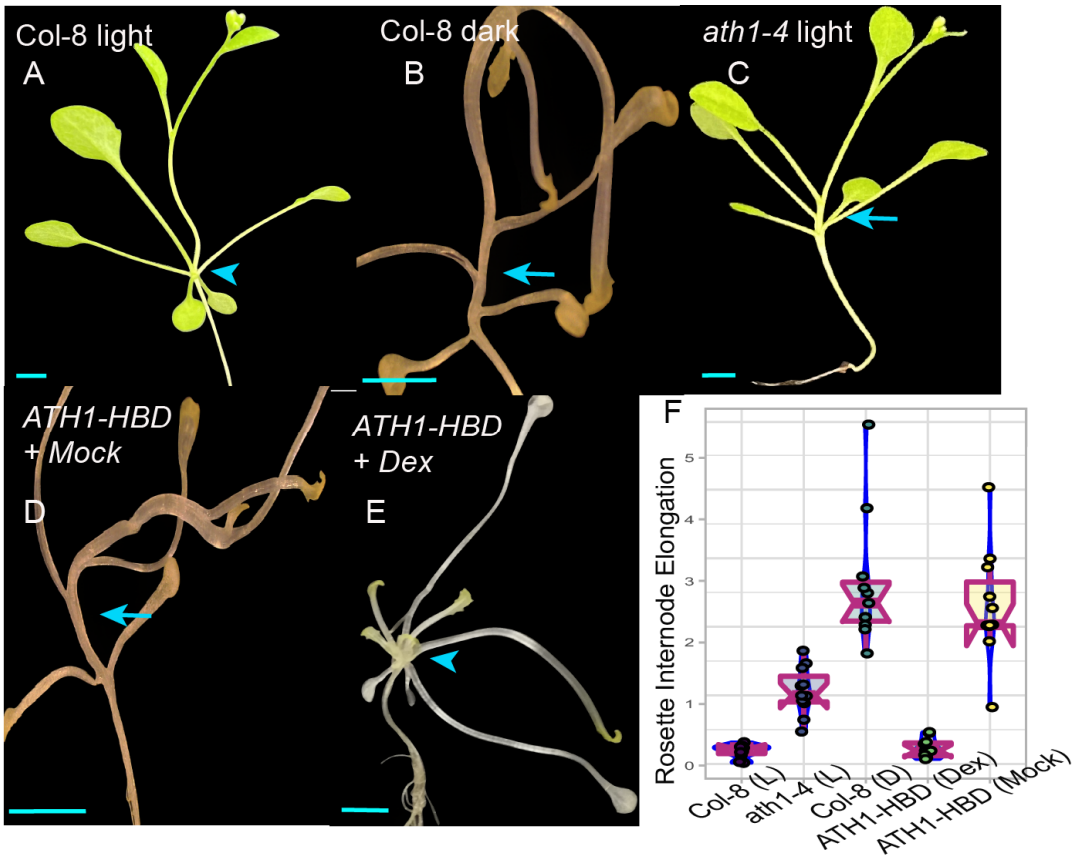

Figure S2: **Sugar-induced dark-grown seedlings phenocopy light-grown *ath1*mutants**
Rosette elongation phenotypes of wild-type Col-8 (**A** and **B**) *ath1-4* (**C**), and *35Spro:ATH1-HBD* (*ATH1-HBD*; **D** and **E**) plants grown in the presence (**A**, **C**) or absence (**B**, **D**, **E**) of light at 27°C. *35Spro:ATH1-HBD* plants were treated either with a mock (0.1% ethanol, **D**) or 10 µM dexamethasone (Dex, **E**). Dark-grown plants (**B**, **D**, **E**) were supplemented with sucrose to a final concentration of one percent three days after the start of the experiment. Arrows indicate elongated rosette internodes, arrowheads indicate complete suppression of internode elongation. **F:** Average rosette internode lengths of plants depicted in **A**-**E**. Per genotype and treatment 10 individual plants were analyzed. Scale bars represent 5 mm.

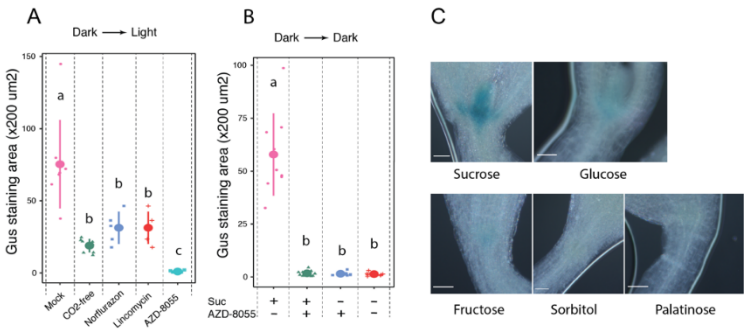

Figure S3: ***ATH1$_{pro}$:GUS*** **activity in seven-day-old seedlings grown in darkness in the presence of different sugars**

A, B: Quantification of GUS-staining intensity in *ATH1$_{pro}$:GUS* shoot apices from **Figure 5B, E**. Different letters denote statistically significant differences between groups ($p < 0.05$) as determined by 1-way ANOVA followed by Tukey's post hoc test.

C: Shoot apices of GUS-stained *ATH1$_{pro}$:GUS* seedlings grown in continuous darkness for seven days. Plants were grown in the presence of either sucrose, glucose, fructose, palatinose, or sorbitol, all added to the growth medium to a final concentration of one percent at the start of the experiment. Scale bars represent 0.05 mm.

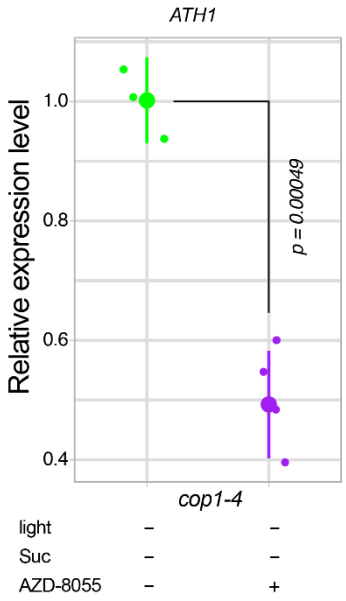

Figure S4: **Effect of TOR inhibition on *ATH1* expression in *cop1-4* mutant seedlings.**
Relative expression of *ATH1* in seven-day-old *cop1-4* mutants grown according to the experimental setup indicated in **Figure 5A**. Seeds were light-treated for 45 minutes to stimulate germination and then grown in continuous darkness for five days. Following the addition of AZD-8055, the seedlings were grown for two more days in darkness before samples were taken. Transcript levels were normalized to *MUSE3* (AT5G15400). The average of three (AZD-8055 -) or four (AZD-8055 +) biological replicates is shown. At least 30 seedlings were used for each biological replicate. The p-value of significant difference, as determined by the two-tailed Student's t-test, is indicated in the figure.